Construction and Building Materials 332 (2022) 127269

Contents lists available at ScienceDirect

Construction and Building Materials

journal homepage: www.elsevier.com/locate/conbuildmat

Residual seismic capacity of beam-column components with corroded reinforcement

Eyitayo A. Opabola

Department of Civil, Environmental and Geomatics Engineering, University College London, London, United Kingdom

ARTICLE INFO

Keywords:
Corrosion
Deterioration
Residual seismic capacity
Concrete structures
Beam-column component

ABSTRACT

Several concrete structures in tectonically active regions of the world are exposed to chloride ingress from seawater, saltwater, and other sources, making them vulnerable to corrosion-induced deterioration. Although it is well-known that corrosion-induced deterioration influences the force-displacement behaviour of corroded concrete components under cyclic loading, no adequate provisions have been incorporated into state-of-practice seismic assessment procedures to account for the influence of corrosion on the modeling parameters and acceptance criteria for concrete components. Using an extensive database of 418 material-level and 271 component-level test specimens with deformed bars, this paper presents simple formulations for evaluating the residual yield strength, ultimate strength, ultimate strain capacity, and bond strength of corroded deformed bars. Conclusions from the material-level study are then used in proposing approaches for predicting the flexural strength, shear strength and failure mode of beam-column components with corroded deformed bars. Subsequently, a simple reduction factor formulation is proposed for predicting corrosion-induced deformation capacity deterioration in corroded concrete components. The proposed reduction factor is demonstrated to be applicable to current deformation capacity formulations in ASCE/SEI 41–17 and Eurocode 8.

1. Introduction

Civil infrastructures are exposed to aggressive environmental conditions (such as concrete carbonation and chloride ingress) during their life-cycle. Such aggressive conditions may result in the corrosion of embedded steel reinforcement. Corrosion propagation in RC components usually results in reduced steel cross-section, cracking and delamination of concrete cover and bond deterioration [1–3]. A large number of buildings and bridges in tectonically active coastal regions are prone to corrosion attacks. Hence, from a seismic assessment perspective, it is essential to ensure the availability of efficient seismic assessment procedures to evaluate the response of corroded concrete components.

Current seismic assessment standards (e.g. ASCE/SEI 41–17 [4] and Eurocode 8 [5]) do not make provisions for evaluating the probable performance of corroded RC components. One of the reasons for the lack of codified provisions for assessing corroded components may be the lack of experimental data and knowledge on the cyclic behaviour of corroded components. However, several component- and material-level tests have been carried out in recent years to fill this gap.

At the component level, studies [6–10] have looked at the influence of uniform and non-uniform corrosion of longitudinal and transverse reinforcement on strength, ductility and failure mode of concrete components. Available test data on the cyclic response of corroded beam-column components have highlighted the significant corrosion-induced reduction in peak lateral strength and deformation capacity at lateral failure. It is also noteworthy that some of the aforementioned studies also looked at retrofitted corroded components. Retrofitted components are, however, outside the scope of the current study. At the material level, studies [1,2,11,12] have discussed the adverse influence of corrosion on the concrete-rebar bond of embedded bars, yield and ultimate strengths, and ultimate strain capacity of corroded bare bars.

Based on experimental results on corroded components, it has been concluded that codified seismic assessment procedures for pristine components may overestimate the probable strength and deformation capacity of corroded components [13]. It is, therefore, important to develop appropriate seismic assessment procedures to (a) capture the influence of corrosion effect on the failure mode of concrete components; (b) predict the reduction in force–displacement parameters for given corrosion levels in the transverse and longitudinal reinforcement of the corroded concrete component.

Recent studies have proposed methodologies for predicting the

E-mail address: e.opabola@ucl.ac.uk.

https://doi.org/10.1016/j.conbuildmat.2022.127269
Received 2 December 2021; Received in revised form 2 March 2022; Accepted 21 March 2022
Available online 4 April 2022

deformation capacity of concrete columns. Goksu et al. [13] capture the influence of bar corrosion on the ultimate tensile strain capacity of the longitudinal bar in a moment–curvature analysis. The column drift capacity is then estimated from the computed curvature capacity using a plastic hinge length equal to half of the column length. However, it is noteworthy that Goksu et al. [13] do not consider the influence of stirrup corrosion on the failure mode, strength, and deformation capacity of corroded columns. Furthermore, the approach was calibrated using only six test specimens.

The current study seeks to develop formulations for evaluating the residual seismic capacity of beam-column components with corroded reinforcement in terms of strength and deformation capacity. In this study, extensive datasets of 418 material-level (229 bare bars and 189 bond tests) and 271 component-level (102 cyclic and 169 monotonic) tests have been adopted in calibrating simple formulations that can be easily used by practising engineers and researchers in assessing the behaviour of corroded concrete beam-column components with deformed bars. Firstly, formulations for predicting the residual yield strength, ultimate strength, and ultimate strain capacity of bare deformed bars are proposed. Subsequently, a model for predicting the residual bond strength of concrete-embedded corroded bars is proposed. Conclusions from the material-level study are then used in proposing approaches for predicting the flexural strength, shear strength and failure mode of beam-column components. Furthermore, a simple reduction factor formulation is proposed for evaluating the probable reduction in deformation capacity at the lateral failure of beam-column components with corroded deformed bars. Lastly, it is shown that the proposed reduction factor can be applied to current deformation capacity formulations in ASCE/SEI 41–17 and Eurocode 8.

2. Experimental database

One of the first steps in this study was a critical review of experimental and analytical studies on the influence of corrosion on the material- and component-level behaviour. For the purpose of this study, five datasets of test specimens with deformed bars were collected. All five datasets are provided in the Appendix.

Dataset 1 consists of 229 bare bar specimens subjected to monotonic tensile loading [1,2,11,12,14–17]. The distribution of key parameters is presented in Table 1. It is noteworthy that measured yield and ultimate strength of bars are typically reported either in terms of apparent stress f_a (i.e. ratio of measured tensile force F_{corr} to the pristine cross-sectional area of the bar A_b) or effective stress f_e (i.e. ratio of measured tensile force F_{corr} to the average cross-sectional area of the corroded bar $A_{b,corr}$, computed from residual mass and length of the bar). For consistency purposes, the reported residual strength values are in terms of apparent stress.

Dataset 2 consists of 189 concrete-embedded straight deformed bar specimens subjected to monotonic pull-out tests [18–25]. All the test specimens in Dataset 2 suffered bond failure with no bar rupture. The distribution of key parameters is presented in Table 2.

Dataset 3 consists of 36 flexure-controlled singly-reinforced beams with corroded tensile reinforcement under monotonic loading [26,27]. The failure mode of the specimens in this dataset was identified based on the published information. In this study, a specimen is classified as flexure-controlled if no critical diagonal cracking was observed throughout the test. Dataset 3 consists of flexural yielding and bond-dominated components. The distribution of key parameters is presented in Table 3.

Dataset 4 consists of 133 shear-controlled beams with corroded stirrups under monotonic loading [10,28–37]. The beams were classified as shear-controlled if the behaviour is dominated by the initiation and propagation of a critical diagonal failure plane. The dataset consists of 121 doubly-reinforced and 12 singly-reinforced beams. The distribution of key parameters is presented in Table 4.

Dataset 5 consists of 23 corroded beam and 79 corroded column components under cyclic loading [6–9,38–52]. 93 out of the 102 corroded specimens have a corresponding pristine specimen. It is noteworthy that poorly-confined components are not well-represented in the database. Only six of the 102 specimens have a ratio of stirrup spacing to effective depth (s/d) > 0.5. This may be attributed to the fact that poor performance is expected of poorly detailed columns irrespective of the corrosion level. Five column specimens have spliced longitudinal reinforcement. All five specimens are from a single test program [13] and have a provided splice length of $40d_b$. The distribution of key parameters is presented in Table 5.

Based on the literature survey of the experimental tests, a summary of the influence of corrosion on the residual capacity of concrete components is presented in Fig. 1. As shown in Fig. 1, reinforcement corrosion directly reduces reinforcement cross-section and causes volumetric expansion of corrosion products [1,6,53]. Chloride ingress results in localized or pitting corrosion which typically concentrates at a point or small area of the reinforcement, while uniform corrosion is typically associated with carbonation [3]. The reduction in reinforcement cross-section, pit formation, and stress concentration negatively influences the stress–strain behaviour (i.e., strength and ductility) of the corroded bar [1,2,16]. The volumetric expansion of the corrosion products results in cracking and delamination of concrete cover [6,8]. The combined effect of concrete cover cracking and reduction in reinforcement cross-section leads to degradation of the concrete-rebar bond [21,22]. Corrosion-induced modification of concrete and steel properties influences the failure mode, stiffness, strength and deformation capacity at the component level [10,26,48,54]. Subsequent sections in this study seek to develop approaches for predicting the failure mode, residual strength, and deformation capacity of corroded components.

Table 1
Distribution of key parameters in the collated bare bars database (Dataset 1).

Parameter	Mean	Maximum	Minimum
Diameter of pristine bar d_b (mm)	15	29	6.5
Yield strength of pristine bar f_y (MPa)	439	550	250
Ultimate strength of pristine bar f_u (MPa)	580	400	666
Ultimate strain capacity of pristine bar ε_u	0.12	0.21	0.1
Mass loss (%)	15.2	82.4	0

Table 2
Distribution of key parameters in the collated pull-out test database (Dataset 2).

Parameter	Mean	Maximum	Minimum
Diameter of pristine bar d_b (mm)	14	20	10
Yield strength of pristine bar f_y (MPa)	442	460	315
Concrete compressive strength f'_c (MPa)	29.8	41	17.7
Concrete cover to bar diameter ratio (c/d_b)	4	7.5	1
Mass loss (%)	5	80	0

Table 3
Distribution of key parameters in the collated database of flexure-controlled singly-reinforced beams with corroded tensile reinforcement (Dataset 3).

Parameter	Mean	Maximum	Minimum
Diameter of pristine bar d_b (mm)	9.5	10	8
Yield strength of pristine bar f_y (MPa)	530	570	520
Concrete compressive strength f'_c (MPa)	37	40	27
Mass loss (%)	11.5	30	2.5
Longitudinal reinforcement ratio ρ_L (%)	0.9	1	0.47
Shear span ratio (a/d)	3	5.6	2.3

Table 4
Distribution of key parameters in the collated database of shear-controlled beams with corroded stirrups (Dataset 4).

Parameter	Mean	Maximum	Minimum
Diameter of pristine bar d_b (mm)	20	25	8
Yield strength of pristine bar f_y (MPa)	456	580	370
Concrete compressive strength f'_c (MPa)	30.7	50	20.7
Tensile longitudinal reinforcement ratio ρ_L (%)	2.3	3.2	0.6
Shear span ratio (a/d)	2.5	4.7	1.55
Mass loss in stirrups (%)	24	97.2	0
Transverse reinforcement ratio ρ_t (%)	0.38	0.9	0.14

Table 5
Distribution of key parameters in the collated database of corroded beam-column components under cyclic loading (Dataset 5).

Parameter	Mean	Maximum	Minimum
Diameter of pristine bar d_b (mm)	19	29	14
Yield strength of pristine bar f_y (MPa)	433	610	355
Concrete compressive strength f'_c (MPa)	32	45	16
Longitudinal reinforcement ratio ρ_L (%)	1.9	3	0.7
Transverse reinforcement ratio ρ_t (%)	0.6	1	0.3
Shear span ratio (a/d)	3.84	11	1.76
Axial load ratio	0.17	0.6	0
Mass loss in stirrups (%)	8	35	0
Mass loss in longitudinal reinforcement (%)	7.5	54	0

3. Influence of corrosion on material and component level behaviour

3.1. Strength of corroded reinforcing bars

Corrosion of the longitudinal and transverse reinforcement in concrete members significantly influence the cyclic response of the concrete members. Various experimental and analytical studies [1,2,11,12,14–17] have been carried to evaluate the influence of corrosion on the stress–strain response of bare reinforcing bars. All experimental programs agree that the yield strength, ultimate strength, and ultimate strain of bare bars are significantly influenced by corrosion.

Du et al. [1] recommend that the residual strength f_{corr} of a corroded bar (having an initial strength f_o) with mass loss of M% can be estimated as:

$$f_{corr} = f_0(1 - 0.005M) \quad (1)$$

Eq. (1) is widely adopted in various studies. It is, however, noteworthy that Eq. (1) suggests that the residual strength of a corroded bar with a mass loss of 100% is $0.5f_o$. Given that Eq. (1) was calibrated to a database with $M \leq 25\%$, Eq. (1) likely provides an unrealistic prediction of residual strength at corrosion levels higher than 25%. Given the extensive database available for this study, it is essential to assess the adequacy of existing formulations for predicting the residual strength of corroded bars.

As earlier mentioned, tensile test data are typically reported in terms of apparent residual stress f_a (i.e. F_{corr}/A_b) or effective residual stress f_e (i.e. $F_{corr}/A_{b,corr}$). By assuming that $A_{b,corr} = A_b(1 - 0.01\ M)$, the relationship between f_a and f_e is given as:

$$f_e = \frac{f_a}{(1 - 0.01M)} \quad (2)$$

The general formulation for predicting the apparent residual stress of a corroded bar is given as:

$$f_a = f_o(1 - \beta M) \quad (3)$$

where β is a reduction coefficient calibrated to experimental data.

Combining Eqs. (2) and (3):

$$f_e = f_o\frac{(1 - \beta M)}{(1 - 0.01M)} \quad (4)$$

The residual tensile force capacity F_{corr} can be evaluated from Eq. (3) as f_aA_b or from Eq. (4) as $f_eA_{b,corr}$.

The recommended value of β by different researchers [15,16,55] ranges from 0.011 – 0.014. Fig. 2a and Table 6 explore the adequacy of recommended β values. As shown in Fig. 2 and Table 6, the best estimate of apparent residual stress is achieved using a β value of 0.013.

It is noteworthy that, based on the definition provided by Du et al. [1], Eq. (1) is defined in terms of effective residual stress. Fig. 2b presents the relationship between the measured f_e/f_o and mass loss. As shown in Fig. 2b, Eq. (1) may overestimate the residual stress at high corrosion levels. Hence, adopting a single coefficient (e.g. Eq. (1)) in predicting the effective residual stress may not be appropriate at high corrosion levels (i.e. M > 50%). In comparison, the more refined Eq. (4), using a β = 0.013, can capture the strength deterioration at high corrosion levels.

Fig. 3 and Table 7 explore the adequacy of the typically recommended β values in predicting the ultimate strength of corroded bare bars. As shown in Fig. 3 and Table 7, similar conclusions can be derived in terms of predicting the ultimate strength of bare bars. Hence, a β value of 0.013 is recommended for predicting the residual yield and ultimate strength of corroded bare bars.

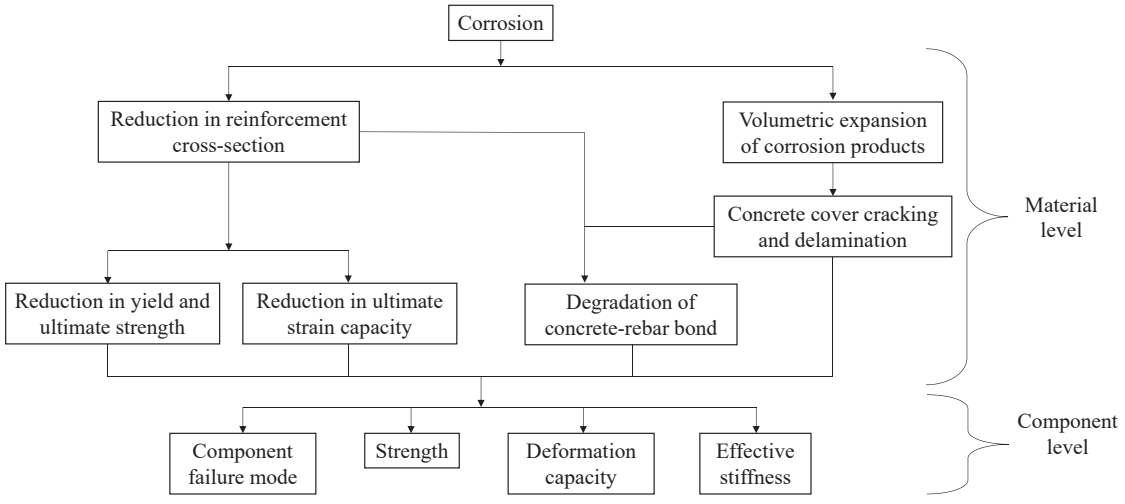

Fig. 1. Influence of corrosion on seismic residual capacity of concrete components.

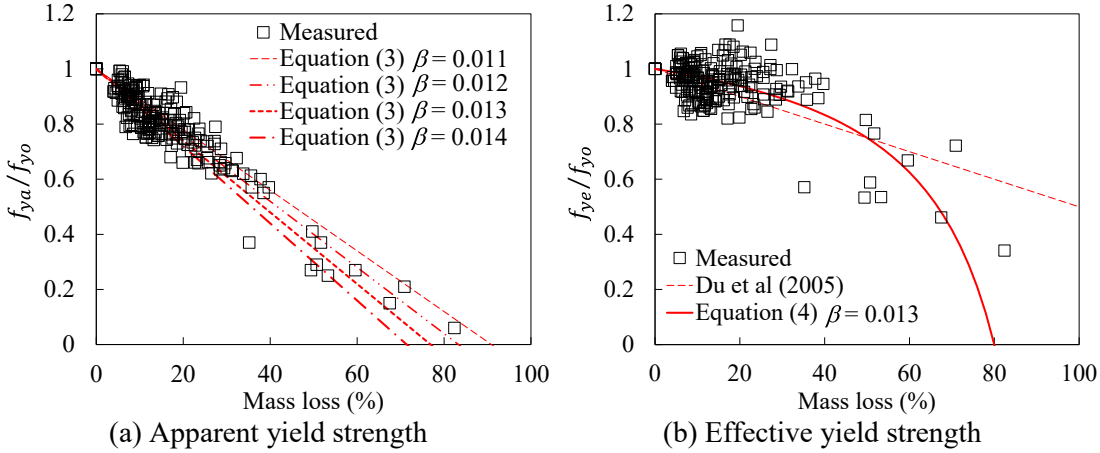

Fig. 2. Influence of mass loss on residual (a) apparent yield strength (b) effective yield strength of bare bars.

Table 6
Adequacy of typically recommended β for predicting the yield strength of corroded bars.

β	Ratio of measured-to-calculated		
	Mean	Median	Coefficient of variation (%)
0.011	0.96	1.00	8.6
0.012	0.98	1.01	7.7
0.013	1.0	1.0	7.7
0.014	1.04	1.0	14.2

3.2. Ultimate strain of reinforcing bars

The influence of corrosion on the ultimate strain capacity of reinforcing bars is explored using Dataset 1. Out of the 229 bare bar tests in Dataset 1, only 105 tests provided data on the measured ultimate strain capacity. Fig. 4 depicts the influence of mass loss on the measured residual ultimate strain capacity of the bare bars in Dataset 1. As shown in the Figure, there is a significant relationship between mass loss and ultimate strain capacity. Various studies have proposed formulations to define this relationship. Du et al. [56] proposed that the residual ultimate strain capacity of a corroded bar ($\varepsilon_{u,corr}$) can be estimated as:

$$\varepsilon_{u,corr} = \varepsilon_{uo}(1 - 0.03M) \quad (5)$$

where ε_{uo} is the ultimate strain capacity of a pristine bar.

Goksu et al. [13] proposed that $\varepsilon_{u,corr}$ can be estimated as:

$$\varepsilon_{u,corr} = \begin{cases} \varepsilon_{uo} \text{ if } M \leqslant 9\% \\ (1.79 - 0.38lnM)\varepsilon_{uo} \text{ if } M > 9\% \end{cases} \quad (6)$$

The adequacy of Eqs. (5) and (6) is shown in Fig. 4 and Table 8. As shown in Fig. 4, the Du et al. [56] formulation provides good $\varepsilon_{u,corr}$ estimates for mass loss values lower than 20%. For higher mass loss values (i.e. M ≥ 34%), Eq. (5) predicts $\varepsilon_{u,corr}$ equals zero. This conservative assumption is attributed to Eq. (5) being originally developed using a dataset of tests with M<25%. By assuming a lower-bound $\varepsilon_{u,corr}$ estimate of 0.01 for Eq. (5) (i.e., to avoid dividing by zero), Eq. (5) provides a mean ratio of measured-to-calculated of 5.25 with a coefficient of variation of 272% for the whole dataset. However, for a subset of tests with M < 30%, Eq. (5) provides a mean ratio of measured-to-calculated of 1.05 with a coefficient of variation of 63%.

For the whole dataset, the Goksu et al. [13] formulation provides an estimate with a mean ratio of measured-to-calculated of 0.8 with a

Table 7
Adequacy of typically recommended β for predicting the ultimate strength of corroded bars.

β	Ratio of measured-to-calculated		
	Mean	Median	Coefficient of variation (%)
0.011	0.96	0.98	7.0
0.012	0.98	1.0	7.1
0.013	1.0	1.0	7.2
0.014	1.02	1.0	10.0

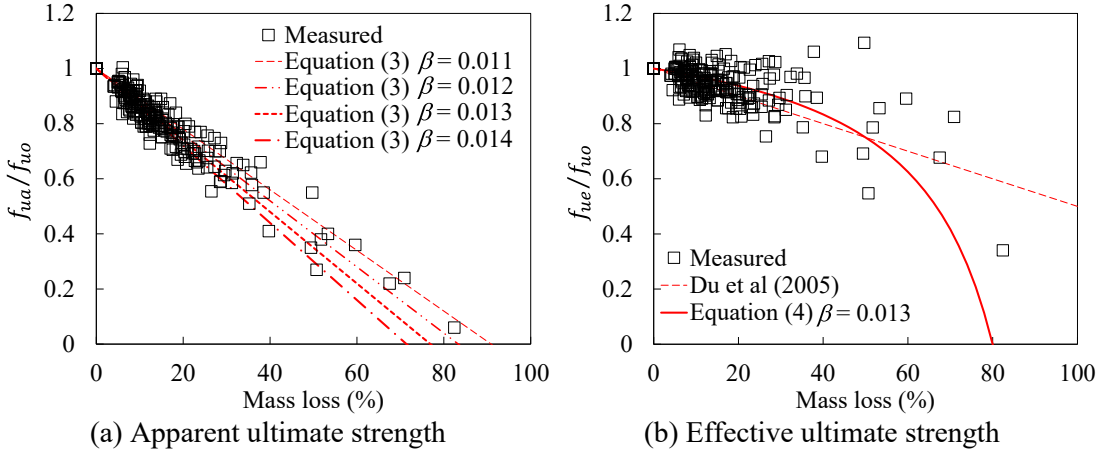

Fig. 3. Influence of mass loss on residual (a) apparent ultimate strength (b) effective ultimate strength of bare bars.

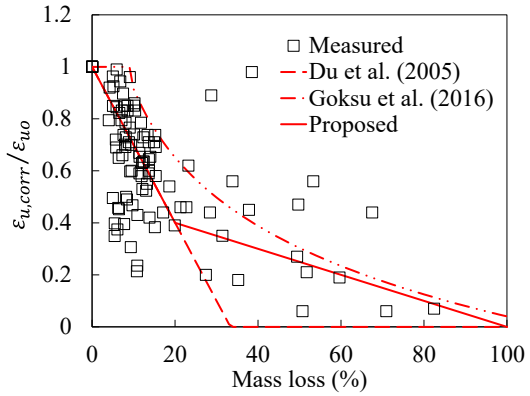

Fig. 4. Influence of mass loss on the residual ultimate strain capacity of corroded bars.

Table 8
Adequacy of formulations for predicting the residual ultimate strain capacity of corroded bars.

Author	Ratio of measured-to-calculated		
	Mean	Median	Coefficient of variation (%)
Du et al. [56]* (all dataset)	5.25	1.0	272
Du et al. [56] (M < 30%)	1.05	1.0	63
Goksu et al. [13] (all dataset)	0.8	0.7	43
Proposed (all dataset)	1.03	1.00	42

*For specimens with M ≥ 34%, a calculated $\varepsilon_{u,corr}$ value of 0.01 was adopted, instead of zero, in order to evaluate the ratio of measured-to-calculated residual ultimate strain capacity of these specimens.

coefficient of variation of 43% (Table 8). As shown in Fig. 4, the Goksu et al. [13] formulation overestimates $\varepsilon_{u,corr}$ across the entire mass loss range.

To address the inadequacies of Eqs. (5) and (6), a formulation fitted to the dataset is proposed as:

$$\varepsilon_{u,corr} = \begin{cases} (1-0.03M)\varepsilon_{uo} \text{ if } M\leqslant 20\% \\ (0.5-0.005M)\varepsilon_{uo} \text{ if } M>20\% \end{cases} \quad (7)$$

As shown in Fig. 4 and Table 8, Eq. (7) provides an estimate with a mean ratio of measured-to-calculated of 1.03 with a coefficient of variation of 42% for the whole dataset. Eq. (7) is recommended for predicting the residual ultimate strain capacity of corroded bars.

3.3. Concrete-rebar bond

The bond mechanism between longitudinal reinforcement and the surrounding concrete is critical to the lateral strength and deformation capacity of concrete components. The required development length of a bar is dependent on the concrete-rebar bond. Available experimental data on pullout tests generally agree that corrosion level below 3% mass loss improves the bond strength of embedded bars. Larger corrosion levels result in a significant reduction in residual bond strength (Fig. 5).

Typically, corrosion-induced expansive radial pressure at the concrete-rebar interface causes the development of hoop tensile stresses in the surrounding concrete. Concrete cracking is initiated once the induced hoop tensile stress exceeds the concrete tensile strength. The mechanical interlock component of the concrete-rebar mechanism is weakened by the concrete cracking, resulting in reduced bond strength of embedded corroded bars.

Various studies have proposed analytical formulations for predicting the residual bond strength of corroded bars not confined by transverse reinforcement. Bhargava et al. [57] proposed that the residual bond strength ($u_{c,corr}$) of a corroded bar not confined by transverse reinforcement can be evaluated as:

$$u_{c,corr} = u_c \cdot 1.192e^{-0.0117M} \leqslant u_c \text{ (MPa)} \quad (8)$$

where u_c is the pristine bond strength.

Chung et al. [22] proposed that the bond strength of a corroded bar not confined by transverse reinforcement can be evaluated as:

$$u_{c,corr} = u_c \cdot 2.09M^{-1.06} \text{ for M} > 2\% \text{ (MPa)} \quad (9)$$

According to Lee et al. [23], the bond strength (τ_{bmax}) of a corroded bar not confined by transverse reinforcement can be evaluated as:

$$u_{c,corr} = 5.21 \cdot e^{-0.0561M} \text{ (MPa)} \quad (10)$$

Eq. (10) assumes that u_c equals 5.21 MPa.

The adequacy of the Bhargava et al. [57], Chung et al. [22] and Lee et al. [23] formulations are explored using the database of pullout tests on corroded bars (Dataset 2). Fig. 5 shows the influence of corrosion-induced mass loss in the embedded deformed bars on the measured bond strength. The adequacy of the discussed formulations is represented in Fig. 5 and Table 9. As shown in Table 9, the Bhargava et al. [57] and Chung et al. [22] formulations provide conservative estimates of the bond strength of corroded bars with a coefficient of variation of 60%. A better estimate of the bond strength of a corroded bar not confined by transverse reinforcement can be derived by fitting a linear formulation to the test data such that:

$$u_{c,corr} = u_c \cdot \gamma_b \leqslant u_c \quad (11)$$

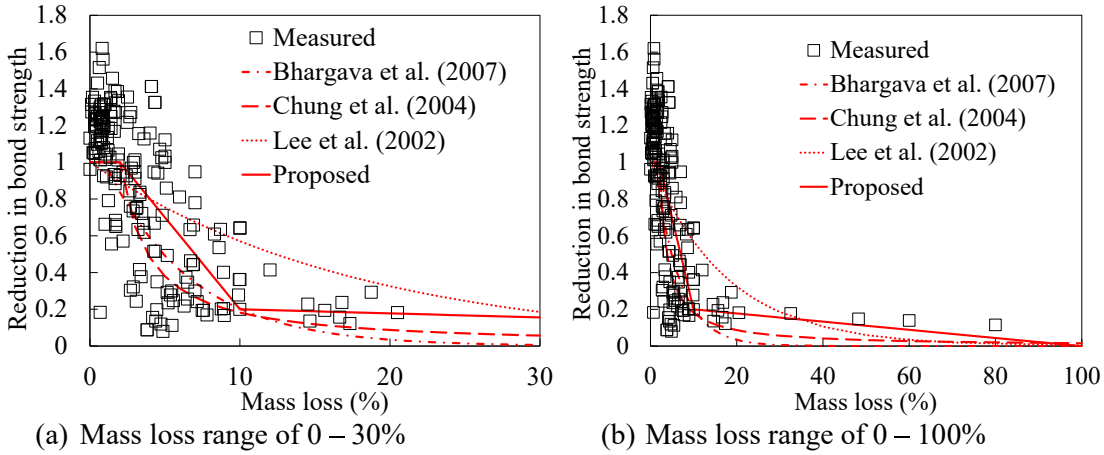

Fig. 5. Influence of mass loss on the bond strength of corroded straight deformed bars.

Table 9
Adequacy of formulations for predicting the bond strength of corroded straight deformed bars.

Author	Ratio of measured-to-calculated		
	Mean	Median	Coefficient of variation (%)
Bhargava et al. [57]	1.33	1.22	60
Chung et al. [22]	1.43	1.23	59
Lee et al. [23]	2.05	1.92	69
Proposed	1.07	1.12	40

where γ_b is the bond reduction factor and is taken as:

$$\gamma_b = \begin{cases} 1 & \text{for M}\leqslant\mathbf{2}\% \\ 0.2 & \text{for M} = \mathbf{10}\% \\ 0 & \text{for M} = 100\% \end{cases} \quad (12)$$

A linear interpolation is required to evaluate for corrosion level between 2 % − 10% and 10% − 100%.

The adequacy of Eq. (12) is presented in Fig. 5 and Table 9. As shown in Table 9, the proposed Eq. (12) provides an estimate with a mean ratio of measured-to-calculated of 1.07 and a coefficient of variation of 40%.

Given the fact that the bond tests were carried out on specimens without stirrups, the effect of stirrup corrosion on the bond strength of corroded tensile bars can not be validated using pullout test data. A simple approach is proposed for predicting the bond strength of corroded longitudinal bars confined by corroded transverse reinforcement. According to Orangun et al. [58], the bond strength of a bar confined by transverse reinforcement (u_b) be represented as the sum of the average bond strength at the failure of the bar not confined by transverse reinforcement (u_c) and the bond strength of the bar attributed to the confinement provided by the transverse reinforcement (u_s). By considering the influence of longitudinal bar corrosion on u_c (i.e., Eq. (11)) and the influence of transverse reinforcement corrosion on u_s, the Orangun et al. [58] can be estimated as:

$$u_{b,corr} = u_{c,corr} + u_{s,corr} = \left[\gamma_c\left(1.2 + 3\frac{c}{d_b} + 50\frac{d_b}{l_a}\right) + \frac{A_{tr,corr}f_{yt,corr}}{3.45nsd_{b,corr}}\right]\frac{\sqrt{f'_c}}{12}, \text{ MPa} \quad (13)$$

where c represents the effective clear cover or clear spacing, l_a is the bar anchorage length $A_{tr,corr}$ is the total cross-sectional area of the corroded transverse reinforcement within spacing s that crosses the potential plane of splitting through the reinforcement being developed, $f_{yt,corr}$ is the residual yield strength of the corroded transverse reinforcement, n and $d_{b,corr}$ are the number and residual diameter of reinforcing bars being developed or lap spliced.

By assuming uniform bond stress along the length of a corroded bar, the development length of a corroded bar $l_{dreq,corr}$ required to develop the residual tensile strength $f_{y,corr}$ of a corroded bar can be derived as:

$$l_{dreq,corr} = \frac{f_{y,corr}d_{b,corr}}{4u_{b,corr}} \quad (14)$$

3.4. Flexural strength

Previous discussions in this paper have focused on material-level behaviour. This section examines the residual flexural capacity of corroded beam-column components under cyclic loading (Dataset 5) and singly- and doubly-reinforced RC beams with corroded tensile bars subjected to three- or four-point monotonic bending tests (Dataset 3). It is noted that all the considered beam-column components in the cyclic database (Dataset 5) experienced flexural yielding. As earlier mentioned, Dataset 3 consists of flexural yielding and bond-dominated components.

The flexural strength of each specimen in Datasets 3 and 5 was evaluated using section analysis. To capture the likelihood of bond failure before flexural yielding, the maximum developable tensile stress in the tensile bars was assessed using the provisions of ASCE/SEI 41–17 [4], replacing the required development length with Eq. (14). A bond failure is expected when the maximum developable tensile stress in the corroded bar $f_{s,corr}$ is lower than the $f_{y,corr}$.

Fig. 6 shows the adequacy of predicting the flexural strength of beams with corroded bars using the adopted methodology. For the monotonic test dataset, the adopted approach provides a flexural strength estimate with a mean measured-to-predicted ratio of 1.02 and a coefficient of variation of 22.7%. For the cyclic test dataset, the adopted approach provides a flexural strength estimate with a mean measured-to-predicted ratio of 1.05 and a coefficient of variation of 24%.

3.5. Shear strength

Various formulations have been proposed for predicting the shear strength of corroded beam components. These formulations are typically based on codified shear strength provisions (e.g. ACI 318 [59], GB50010-2002 [60]) with appropriate modifications to account for concrete damage and steel corrosion effects. To evaluate the shear strength of RC beams, this paper combines the ACI-ASCE Committee 326 [61] formulation for concrete contribution to shear and the traditional formulation for stirrups contribution to shear (Eq. (15)).

$$V_n = V_c + V_s = \left[0.16\sqrt{f'_c} + 17\rho_w\frac{d}{a}\right]bd + \frac{A_v f_{yt}d}{s} \quad (15)$$

Tests on shear-critical singly-reinforced beams without transverse reinforcement are suitable for assessing the influence of corrosion level on the concrete contribution to shear strength. However, such data is scarce. Available experimental data on shear-critical singly-reinforced beams without transverse reinforcement [62] suggest that the shear stress capacity may not be significantly compromised by the corrosion level in the longitudinal reinforcement (See Fig. 7). This can be attributed to the fact that the shear resistance contribution from the concrete in the compression zone and the contribution from the aggregate interlock action along the diagonal failure plane may be significantly larger than the contribution of the dowel mechanism from the longitudinal bars. Hence, the reduced dowel mechanism contribution from the corroded longitudinal reinforcement may not significantly influence the shear strength of the beam. Further testings are needed to validate this conclusion.

Based on the limited available data, it is assumed that the concrete contribution to shear stress capacity is not significantly affected by corrosion. However, it is important to account for concrete section loss from cracking and spalling when estimating the concrete contribution to shear strength. If significant concrete cover delamination is observed, the shear area ($b_{corr}d_{corr}$) can be taken as the area of the concrete core in Eq. (16).

$$V_{n,corr} = V_{c,corr} + V_{s,corr} = \left[0.16\sqrt{f'_c} + 17\rho_w\frac{d_{corr}}{a}\right]b_{corr}d_{corr} + \frac{A_v f_{yt,corr}d_{corr}}{s} \quad (16)$$

The stirrup contribution is evaluated considering corrosion effects on the stirrups. If $f_{yt,corr}$ is taken as the apparent residual strength accounting for the mass loss in the transverse reinforcement (M_t) (i.e., computed using Eq. (3)), A_v is taken as the pristine transverse reinforcement area A_{vo}. If $f_{yt,corr}$ is taken as the effective residual strength (i.e., computed using Eq. (4)), A_v is taken as $A_{vo}(1–0.01M_t)$).

Fig. 8 shows the adequacy of Eq. (16) in predicting the residual shear strength capacity of shear-critical doubly-reinforced beams in Dataset 4. As shown in Fig. 8, Eq. (16) provides a mean measured-to-computed estimate with a 1.17 and coefficient of variation of 25%.

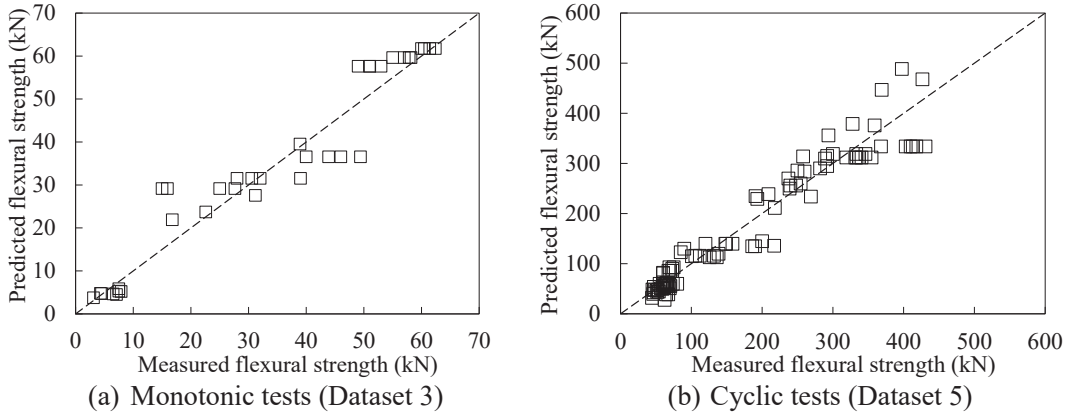

Fig. 6. Predicting the flexural strength of (a) monotonic beam tests (Dataset 3) (b) cyclic beam-column tests (Dataset 5).

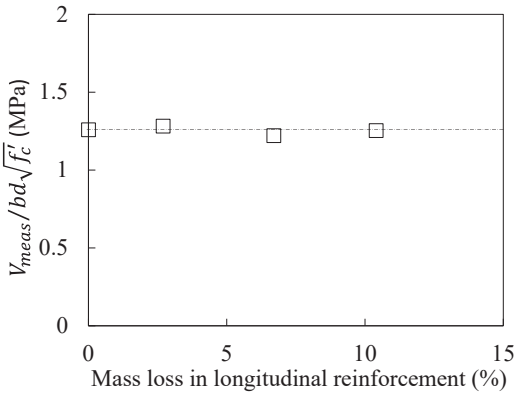

Fig. 7. Influence of longitudinal reinforcement corrosion on measured peak shear stress of nominally identical singly-reinforced beams with varying corrosion levels in the longitudinal reinforcement (Data from [62]).

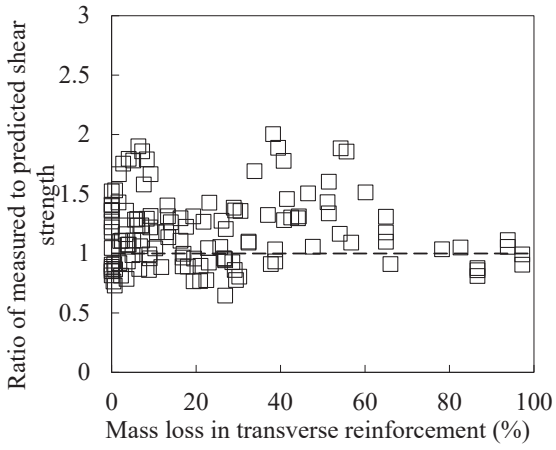

Fig. 8. Adequacy of Eq. (16).

3.6. Failure mode of corroded RC components

Corrosion-induced failure mode switch has been observed in various component tests. Typically observed failure mode switch cases include a switch from a brittle-shear mechanism to a flexure-dominated mechanism [10,54,62], a switch from a flexure-dominated mechanism to a flexure-shear dominated mechanism [47]. Corrosion-induced failure mode switch can be attributed to the influence of corrosion on the shear capacity and flexural strength of the corroded component (i.e. flexure-shear interaction).

For example, Fig. 9a is a hypothetical depiction of the influence of corrosion on flexure-shear interaction in a component, with little or no shear confinement, under monotonic loading. As depicted in Fig. 9a, flexure-shear interaction in the pristine component results in a brittle-shear dominated mechanism in the component. Due to reinforcement corrosion, however, reduction in the flexural ($V_{p,corr}$) and shear ($V_{n,corr}$) capacities of the beam may inhibit flexure-shear interaction, and this results in the corroded component having a higher deformation capacity.

Fig. 9b depicts the occurrence of corrosion-induced activation of flexure-shear interaction as observed in cyclic tests on code-conforming components (e.g. [47]). As shown in Fig. 9b, significant corrosion of the stirrups results in degradation of the undegraded shear strength (i.e. from V_o to $V_{o,corr}$). Also, the longitudinal reinforcement corrosion results in flexural strength degradation from V_p to $V_{p,corr}$. Under cyclic demands, the shear envelope and the flexural curve of the corroded components interact, leading to an undesirable flexure-shear failure mechanism and reduced ductility.

Hence, for adequate prediction of the seismic response of corroded concrete components, the identification of the probable failure mode is important. A proposed flowchart for predicting the failure mode of corroded RC components is presented in Fig. 10. The flowchart has been modified from the failure mode prediction procedure discussed in Opabola and Elwood [63].

The residual flexural strength $V_{p,corr}$ of the corroded component is computed through section analysis using $f_{y,corr}$ as previously discussed in this paper. Modified component concrete cross-sectional properties should be used if visual assessment suggests deterioration of the concrete cross-section. The flexural strength corresponding to maximum developable tensile stress in the corroded bars $V_{b,corr}$ is calculated using the provisions of ASCE/SEI 41–17, replacing the required development length with Eq. (14). The 'undegraded' shear strength ($V_{o,corr}$) for a corroded column is computed using a modified version of the Sezen and Moehle shear strength model (Eq. (17)).

$$V_{o,corr} = \frac{A_{v,corr} f_{yt,corr} d_{corr}}{s} + \left(\frac{0.5\sqrt{f'_c}}{M/Vd}\sqrt{1+\frac{N}{0.5\sqrt{f'_c}A_{g,corr}}}\right)0.8A_{g,corr} \quad (17)$$

where $A_{g,corr}$ is the residual gross cross-sectional area of the column.

As shown in Fig. 10, the probable failure mode of a corroded RC component is defined by comparing the three calculated strength parameters (i.e. $V_{p,corr}$,$V_{b,corr}$, and $V_{o,corr}$). A shear capacity ratio (i.e. ratio of calculated shear strength $V_{o,corr}$ to the flexural strength $V_{p,corr}$) not less than one is used to classify components as brittle shear-critical. As recommended in ASCE/SEI 41–17, the current study retains a shear

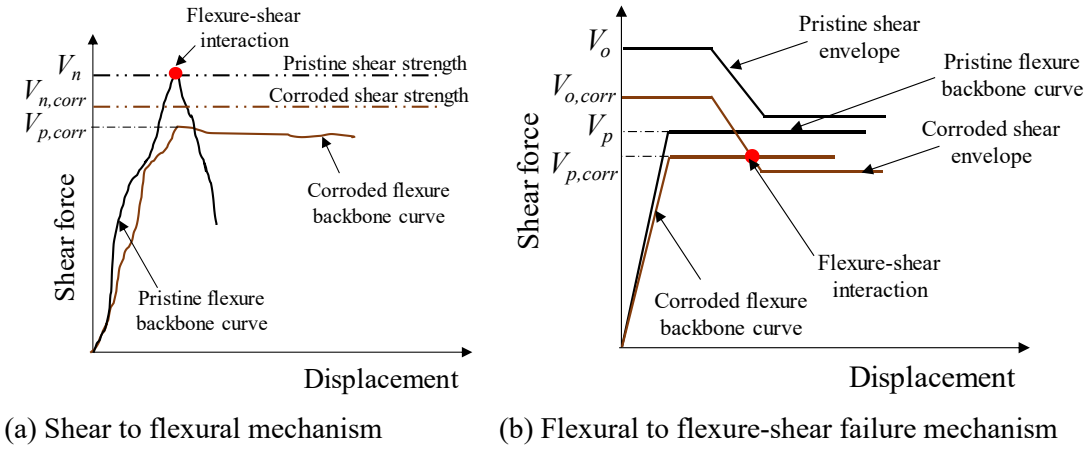

Fig. 9. Influence of bar corrosion on flexure-shear interaction and failure mode switch.

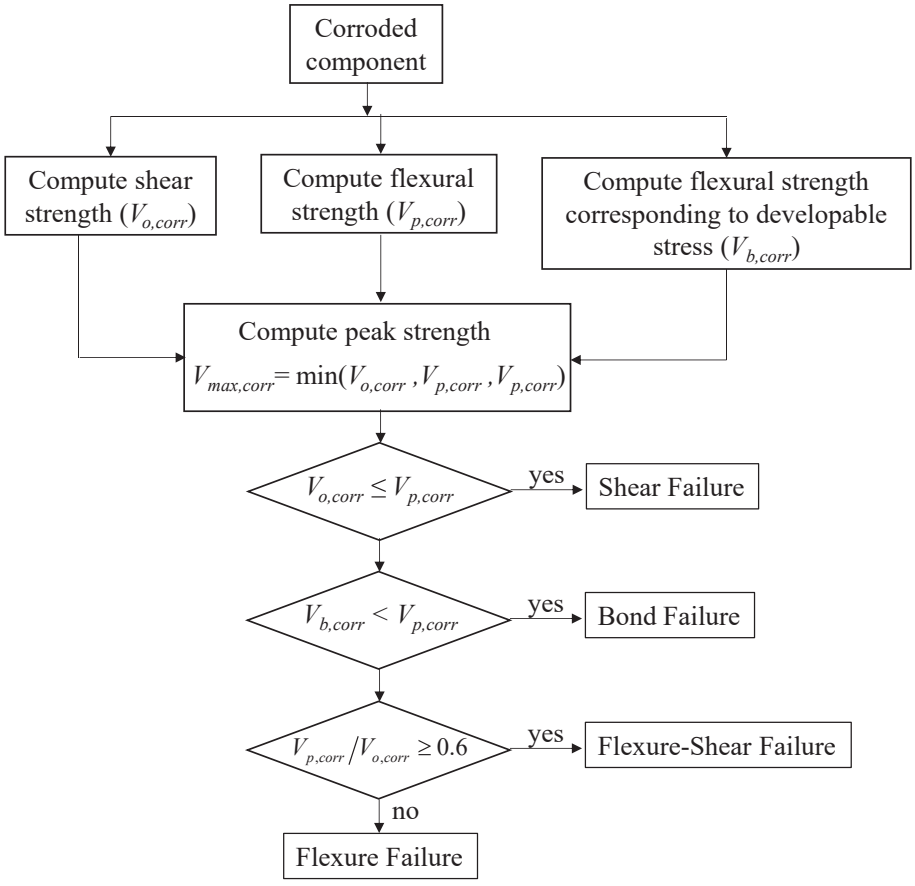

Fig. 10. Flowchart for predicting the failure mode of corroded column components.

capacity ratio of 0.6 as the boundary between flexure and flexure-shear failure modes because currently available test data on corroded components do not suggest the need for any modifications. Apart from using the shear capacity ratio as a failure mode index, even if well-detailed, beam-column components with high shear distress ($\geq 0.3\sqrt{f'_c}$, in MPa units) may be flexure-shear controlled [64].

The observed failure mode of the 102 beam-column specimens in Dataset 5 was compared with the failure mode approach described in this section. The observed failure mode of each component in Dataset 5 was identified using an approach adopted in previous studies [63]. A confusion matrix for this comparison is presented in Table 10. The data along the principal diagonal indicate the number of components whose failure modes were accurately predicted by the proposed approach. The failure mode of 70%, 92%, and 92% of the flexure, flexure-shear, and shear-controlled specimens, respectively, were accurately predicted. Data above the principal diagonal indicate conservative failure mode classification. For example, "15" indicates that there are 15 flexure-controlled components conservatively classified as flexure-shear. 30% of the flexure-controlled columns were conservatively predicted as flexure-shear while 5% of the flexure-shear columns were conservatively predicted as shear-controlled. On the other hand, the data below the principal diagonal indicate unconservative failure mode classification.

Table 10
Evaluation of failure mode prediction approach for components in Dataset 5.

		Predicted failure mode			
		Flexure	Flexure-shear	Shear	**Total**
Observed failure mode	Flexure	35	15	0	**50**
	Flexure-shear	1	37	2	**40**
	Shear	0	1	11	**12**
	Total	**36**	**53**	**13**	**102**

As shown in Table 10, only one shear-controlled column was unconservatively classified as flexure-shear. In general, the failure mode classification accurately predicts the failure mode of 81% of the test specimens.

3.7. Deformation capacity at lateral failure

This section explores the influence of reinforcement corrosion on the deformation capacity at lateral failure of concrete beam-column components subjected to cyclic loading (Dataset 5). Three deformation quantities were extracted from the force–displacement plots of each test specimen – (a) the yield rotation (θ_y) was estimated by drawing a secant line from the origin to pass through the backbone curve at 70% of the maximum lateral load (V_{max}) and made to intersect the horizontal line corresponding to V_{max} (b) the drift capacity at lateral failure (θ_u) is defined as the drift corresponding to a 20% drop in lateral strength (c) the plastic rotation capacity (θ_p) defined as the difference between the measured yield rotation and drift capacity.

The collated Dataset 5 was binned into three groups: Group A consists of test specimens in which only the longitudinal reinforcement was corroded; Group B consists of test specimens in which only the transverse reinforcement was corroded; and Group C consists of test specimens in which both the longitudinal and transverse reinforcement were corroded.

As previously mentioned, 93 out of the 102 corroded specimens have a corresponding pristine specimen. For the specimens in the collated dataset with a corresponding nominally identical pristine specimen, the ratio of deformation capacity of the corroded specimen to the pristine specimen was computed. Two deformation capacity ratios were computed – the first in terms of drift capacity ($\theta_{u,corr}/\theta_{u,uncorr}$) and the second in terms of plastic rotation capacity ($\theta_{p,corr}/\theta_{p,uncorr}$).

Fig. 11 and Fig. 12 show the influence of corrosion level on the drift capacity of specimens in Group A and Group B, respectively. The influence of longitudinal reinforcement on the deformation capacity, as shown in Fig. 11, can be attributed to a reduction in the tensile strain capacity of the corroded bars. The reduction in the deformation capacity of components in Group B, as shown in Fig. 12, is attributed to the reduced confinement effect of the transverse reinforcement as the corrosion level increases. Apart from the influence of the reduced confinement on the shear capacity, the deteriorated stirrups are unable to constrain the longitudinal reinforcement effectively, resulting in an early onset of longitudinal reinforcement buckling and degradation of the concrete core.

As shown in Fig. 11 and Fig. 12, the available experimental data suggest that the segregated influence of corrosion level of longitudinal reinforcement and transverse reinforcement can be expressed using a linear relationship as a function of mass loss. The reduction factor to deformation capacity due to corrosion of longitudinal reinforcement only (ψ_l) can be estimated as:

$$\psi_l = \frac{\theta_{u,corr\_groupA}}{\theta_{u,uncorr\_groupA}} = \frac{\theta_{p,corr\_groupA}}{\theta_{p,uncorr\_groupA}} = 1 - 0.017M_l \tag{18}$$

where M_l is the mass loss in the longitudinal reinforcement (in percent). For the test specimens in Group A, Eq. (18) provides an estimate with a mean ratio of measured to computed plastic rotation capacity of 1.0 and a coefficient of variation of 24%.

The reduction factor to deformation capacity due to corrosion of transverse reinforcement only ($\psi_{l=t}$) can be estimated as:

$$\psi_t = \frac{\theta_{u,corr\_groupB}}{\theta_{u,uncorr\_groupB}} = \frac{\theta_{p,corr\_groupB}}{\theta_{p,uncorr\_groupB}} = 1 - 0.022M_t \tag{19}$$

where M_t is the mass loss in the transverse reinforcement (in percent). Eq. (19) provides an estimate with a mean ratio of measured to computed plastic rotation capacity of 1.0 and a coefficient of variation of 26%.

Furthermore, available experimental data were studied to assess the likelihood of a higher level of corrosion-induced deformation capacity degradation with increased axial load. Test specimens in Group A and B were further subdivided into smaller bins based on mass loss in the reinforcement (See Fig. 13 a & b). As shown in Fig. 13 a & b, currently available data do not suggest any higher level of corrosion-induced deformation capacity degradation with increased axial load. Fig. 13c shows the influence of axial load on the reduction in deformation capacity for the entire database. As shown in Fig. 13c, no significant trend is observed.

The test specimens in Group C were then used in assessing the combined influence of longitudinal and transverse reinforcement corrosion on the reduction in deformation capacity (i.e. ($\theta_{p,corr\_groupC}/\theta_{p,uncorr\_groupC}$)). Firstly, an assumption was made that:

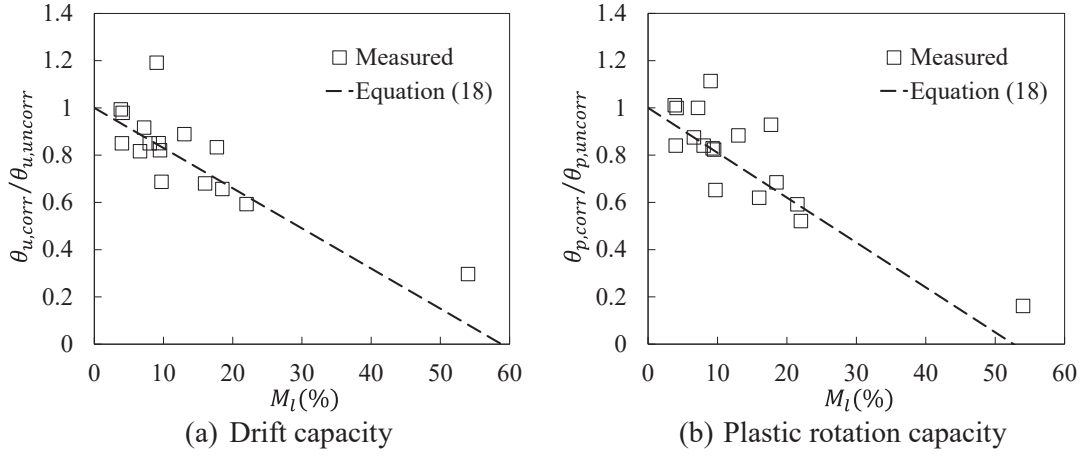

Fig. 11. Influence of longitudinal reinforcement corrosion level (M_l) on (a) drift capacity (b) plastic rotation capacity of beam-column components in Group A.

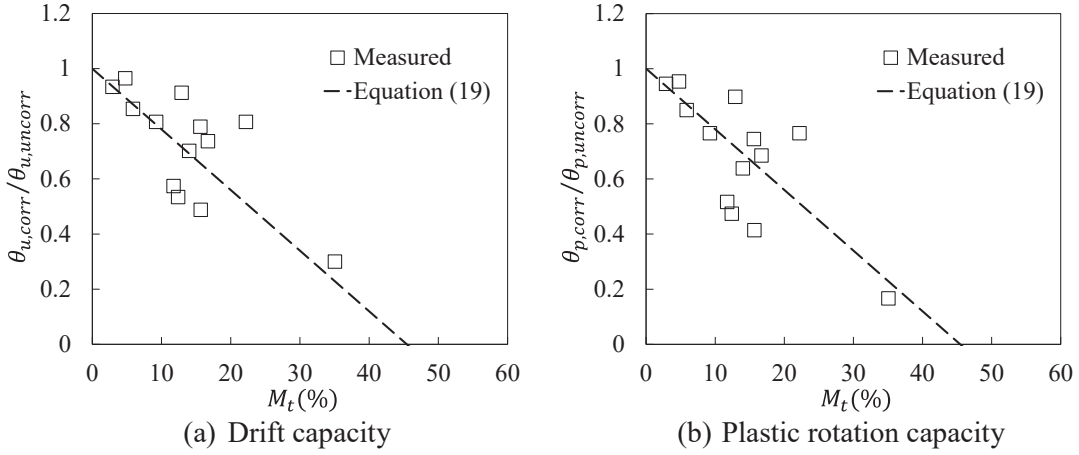

Fig. 12. Influence of transverse reinforcement corrosion level (M_t) on (a) drift capacity (b) plastic rotation capacity of beam-column components in Group B.

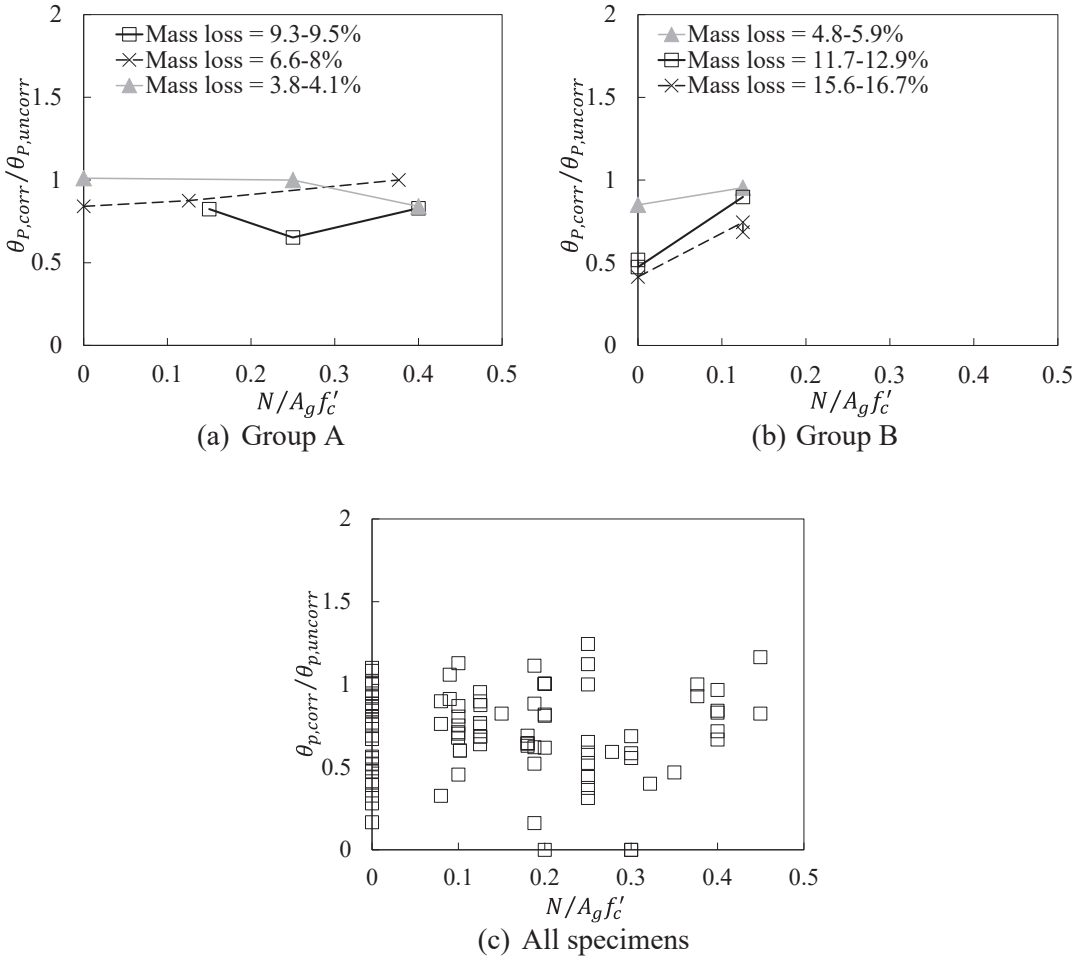

Fig. 13. Influence of axial load ratio on the corrosion-induced reduction factor.

$$\frac{\theta_{p,corr\_groupC}}{\theta_{p,uncorr\_groupC}} = f(\psi_l, \psi_t) \tag{20}$$

Following Eq. (18), it was assumed that the relationship between ψ_l and $\theta_{p,corr\_groupC}/\theta_{p,uncorr\_groupC}$ is linear, such that the relationship between ψ_t and $\theta_{p,corr\_groupC}/\theta_{p,uncorr\_groupC}$ can be evaluated by comparing the ratio of measured $\theta_{p,corr\_groupC}/\theta_{p,uncorr\_groupC}$ to the computed ψ_l (using Eq. (18)) of each specimen in Group C. Fig. 14 shows the relationship between the ratio of measured $\theta_{p,corr\_groupC}/\theta_{p,uncorr\_groupC}$ to computed ψ_l and the mass loss in the transverse reinforcement of the specimens in Group C. As shown in Fig. 14, the trendline of ($\theta_{p,corr\_groupC}/\theta_{p,uncorr\_groupC}$)/ ψ_l can be expressed using Eq. (19).

Hence, the reduction factor η to the deformation capacity of a corroded beam-column component can be estimated as:

$$\eta = \frac{\theta_{p,corr}}{\theta_{p,uncorr}} = \psi_l \psi_t \tag{21}$$

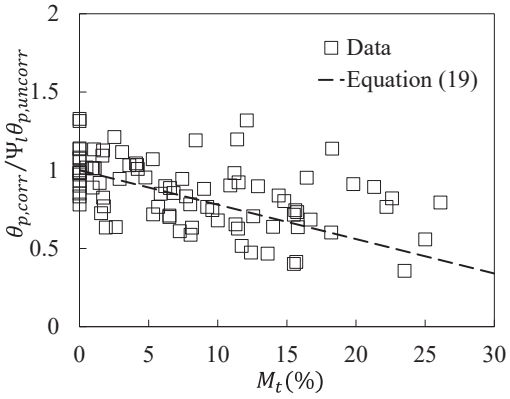

Fig. 14. Relationship between the ratio of measured $\theta_{p,corr\_groupC}/\theta_{p,uncorr\_groupC}$ to computed ψ_l and the mass loss in the transverse reinforcement.

where ψ_l and ψ_t are computed using Eqs. (18) and (19) respectively.

The adequacy of Eq. (21) is shown in Fig. 15 as a function of axial load ratio. For all the specimens in the database, Eq. (21) provides an estimate with a mean ratio of measured to computed reduction factor of 1.1 and a coefficient of variation of 27.1%.

Fig. 16 presents the range of reduction factors computed using Eq. (21) for longitudinal (M_l) and transverse reinforcement (M_t) corrosion levels ranging from zero to 60%. As shown in Fig. 16, the residual deformation capacity of corroded concrete beam-column component degrades below 50% when transverse reinforcement corrosion levels exceed 20%.

A key limitation of the current study is that Eq. (21) has been calibrated with data on flexure-, flexure-shear and shear-controlled beam-column components. Experimental test data are needed to validate the applicability of Eq. (21) to bond-controlled components. In the absence of such experimental data, appropriate modifications can be made to formulations for predicting the deformation capacity of bond-controlled components (e.g., [63,65]).

The deformation capacity of a corroded specimen can be computed by replacing $\theta_{p,uncorr}$ in Eq. (21) with any deformation capacity formulation calibrated to a database of pristine specimens. Adopting the modelling parameter a in ASCE/SEI 41–17 for columns, the plastic rotation capacity at lateral failure for a corroded column specimen not controlled by inadequate development or splicing of longitudinal reinforcement is estimated as:

$$a_{corr} = \eta\left[0.042 - 0.043\frac{N}{A_g f_c'} + 0.63\rho_t - 0.023\frac{V_p}{V_o}\right] \text{ for rectangular components}$$

$$a_{corr} = \eta\left[0.06 - 0.06\frac{N}{A_g f_c'} + 1.3\rho_t - 0.037\frac{V_p}{V_o}\right] \text{ for circular components} \quad (22)$$

Adopting the plastic rotation capacity model in Eurocode 8:3, the plastic rotation capacity at lateral failure for a corroded specimen can be estimated as:

$$\theta^{pl}_{um,corr} = \frac{\eta}{\gamma_{el}} 0.0145\cdot(0.25^{\nu})\left[\frac{max(0.01;w')}{max(0.01;w)}\right]^{0.3} f_c'^{0.2}\left(min\left(9;\frac{L_v}{h}\right)\right)^{0.35} 25^{\left(\alpha\rho_{sx}\frac{f_{yw}}{f_c'}\right)}(1.275^{100\rho_d}) \quad (23)$$

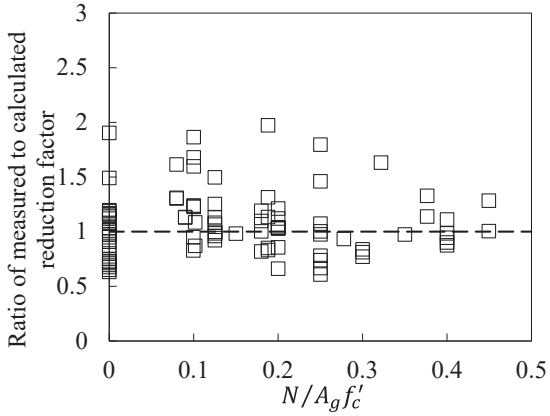

Fig. 15. Adequacy of Eq. (21) for all beam-column components.

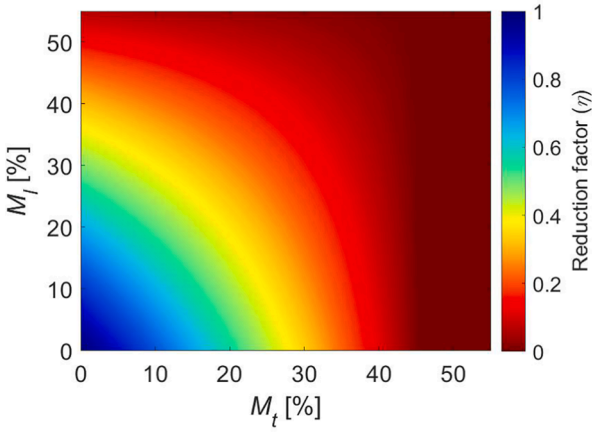

Fig. 16. Reduction factors for various corrosion levels in longitudinal (M_l) and transverse reinforcement (M_t).

where γ_{el} equals 1.8 and 1.0 for primary and secondary seismic members respectively (This coefficient is meant to convert mean values of ultimate rotation to 'mean minus one standard deviation'); h: is the depth of cross-section; L_v is shear span; ν is axial load ratio; ω and ω' are mechanical reinforcement ratio of tension and compression bars; f'_c is the concrete compressive strength in Mpa; f_{yw} is the steel yield strength in Mpa; ρ_{sx} is the transverse reinforcement ratio; α is the confinement effectiveness factor, and ρ_d is the steel ratio.

Fig. 17a shows the adequacy of Eq. (22). Eq. (22) provides an estimate with a mean ratio of measured to computed plastic rotation capacity at lateral failure of 1.3 and a coefficient of variation of 35%.

Fig. 17b shows the adequacy of Eq. (23). $\gamma_{el} = 1.0$ was adopted to get a mean estimate. Eq. (23) provides an estimate with a mean ratio of measured to computed plastic rotation capacity at lateral failure of 0.98 and a coefficient of variation of 30%. It is noted that the higher level of dispersion in Fig. 17 in comparison to Fig. 15 can be attributed to uncertainty in the ASCE/SEI 41–17 and Eurocode 8 formulations.

4. Conclusion

Corrosion-induced deterioration influences the failure mode, strength and deformation capacity of concrete components. Corrosion-induced deterioration can switch the failure mode of a well-confined

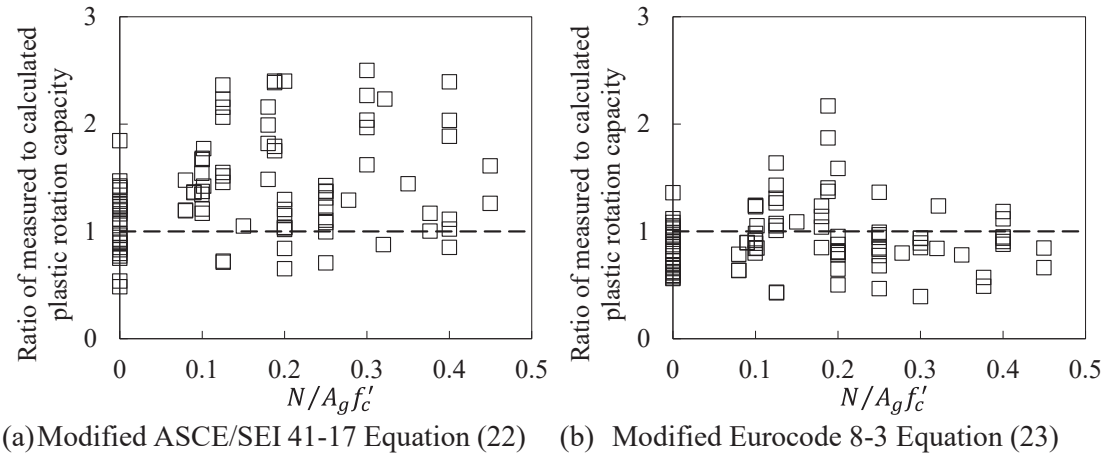

Fig. 17. Adequacy of (a) Eq. (22) (b) Eq. (23) for all beam-columns in Dataset 5.

component to an undesirable shear-dominated response. Also, the strength and deformation capacity of concrete components are adversely affected by corrosion. Despite the influence of corrosion-induced deterioration on the residual seismic response of concrete components, there are currently no seismic assessment provisions for corroded concrete components. To address these concerns, this paper has developed a seismic assessment procedure for assessing the failure mode and force–displacement response of corroded beam-column components.

Firstly, an extensive database of laboratory tests of 418 material- (229 bare bars and 189 pullout tests) and 271 component-level (102 cyclic and 169 monotonic) corroded specimens with deformed bars was developed. Key variables in the database include corrosion level in transverse and longitudinal reinforcement, transverse reinforcement detailing of components, axial load ratio on components, aspect ratio and concrete strength.

The extensive dataset of bare bar tests was adopted in evaluating the adequacy of typically recommended reduction coefficients (β) to compute the residual strength of bare bars. It was concluded that a β –factor of 0.013 is the most appropriate, provided a yield strength estimate with a mean ratio of measured-to-calculated of 1.0 and coefficient of variation of 7.7%. The β –factor of 0.013 provides an ultimate strength estimate with a mean ratio of measured-to-calculated of 1.0 and coefficient of variation of 7.2%. Using data from the bare bar tests, a formulation was proposed to predict the ultimate strain capacity of corroded bars. The proposed formulation provides an estimate with a mean ratio of measured-to-calculated of 1.03 and coefficient of variation of 42%. The monotonic pullout test dataset was used to develop a formulation for predicting the residual bond strength of a corroded bar. The proposed equation provides an estimate with a mean measured-to-calculated ratio of 1.1 and a coefficient of variation of 40%.

The recommended approach for evaluating the shear strength of doubly-reinforced beams provide an estimate with a mean measured-to-calculated ratio of 1.17 and coefficient of variation of 25%. The recommended approach for evaluating the flexural strength of corroded beam-column components provide an estimate with a mean measured-to-calculated ratio of 1.02 and coefficient of variation of 22.7% for components under monotonic loading; and an estimate with a mean measured-to-calculated ratio of 1.05 and coefficient of variation of 24% for components under cyclic loading.

Using the component-level datasets, simple approaches were proposed for predicting the failure mode and force–displacement parameters of concrete beam-column components. The proposed failure mode classification approach captures the likelihood of flexure-, flexure-shear, shear- and bond-dominated mechanisms in the components. The failure mode classification approach accurately predicts the failure mode of 81% of the 102 cyclic test specimens.

This paper proposes a simple reduction factor formulation to predict the deformation capacity of corroded components as a function of the corrosion levels in transverse and longitudinal reinforcement. The proposed reduction factor can be applied to existing deformation capacity formulations developed for pristine components. Applying the reduction factor to the Eurocode 8 provisions, the proposed approach provides a plastic rotation capacity estimate with a mean ratio of measured to computed plastic rotation capacity at lateral failure of 0.98 and a coefficient of variation of 30%. Applying the reduction factor to the ASCE/SEI 41–17 provisions, the proposed approach provides a plastic rotation capacity estimate with a mean ratio of measured to computed plastic rotation capacity at lateral failure of 1.3 and a coefficient of variation of 35%.

CRediT authorship contribution statement

Eyitayo A. Opabola: Conceptualization, Methodology, Writing – original draft, Writing – review & editing.

Declaration of Competing Interest

The authors declare that they have no known competing financial interests or personal relationships that could have appeared to influence the work reported in this paper.

Appendix

Dataset 1 – Tensile tests on bare corroded bars.

Author	Specimen name	d_{b0} (mm)	Mass loss (%)	f_{yexp} (MPa)	f_{uexp} (MPa)	$e_{u,exp}$
Moreno et al. [2]	R-d16	16	0.0	540.92	649.10	0.107
	B-1	16	4.0	517.48	632.38	0.085
	B-2	16	5.0	533.83	636.94	0.103
	B-3	16	5.1	531.03	652.92	0.099
	B-4	16	5.9	522.49	631.30	0.090
	B-5	16	6.6	562.10	672.61	0.088
	B-6	16	6.8	458.25	616.56	0.101
	B-7	16	7.1	528.21	640.84	0.085
	B-8	16	7.1	522.74	644.30	0.089
	B-9	16	7.4	525.66	645.23	0.096
	B-10	16	7.6	505.82	634.05	0.079
	B-11	16	7.9	530.27	633.08	0.075
	B-12	16	7.9	552.80	665.58	0.091
	B-13	16	8.0	543.22	642.55	0.074
	B-14	16	8.1	498.06	616.13	0.084
	B-15	16	8.1	469.30	610.62	0.078
	B-16	16	8.5	550.14	653.04	0.089
	B-17	16	8.8	470.87	602.29	0.076
	B-18	16	9.0	518.06	635.85	0.082
	B-19	16	9.1	528.90	647.80	0.103
	B-20	16	9.2	554.11	658.14	0.064
	B-21	16	9.7	537.09	619.20	0.050
	B-22	16	10.1	523.57	626.51	0.091
	B-23	16	10.4	474.75	582.36	0.089
	B-24	16	11.4	518.06	637.48	0.072
	B-25	16	11.4	458.97	578.87	0.070
	B-26	16	11.8	469.32	616.48	0.084
	B-27	16	11.9	495.85	591.00	0.062
	B-28	16	12.3	517.40	617.62	0.068
	B-29	16	12.4	491.95	593.73	0.078
	B-30	16	12.4	512.10	609.23	0.068
	B-31	16	13.0	504.37	594.38	0.056
	B-32	16	13.3	506.72	621.47	0.079
	B-33	16	13.6	527.68	633.20	0.076
	B-34	16	13.7	514.14	620.42	0.069
	B-35	16	14.0	506.90	622.22	0.070
	B-36	16	15.1	519.30	574.25	0.041
	B-37	16	15.2	521.18	622.61	0.079
	B-38	16	15.3	525.73	643.55	0.074
Ou et al. [15]	N-0	13	0.0	305.60	405.80	0.140
	N-1	13	27.4	332.54	391.27	0.028
	N-2	13	49.4	163.07	280.69	0.038
	N-3	13	49.7	249.10	443.72	0.066
	N-4	13	51.7	234.10	319.26	0.029
	N-5	13	53.3	163.60	347.58	0.078
	N-6	13	59.6	204.24	361.60	0.027
	N-7	13	67.5	141.05	274.70	0.062
	N-8	13	70.9	220.54	334.68	0.008
	N-9	13	82.4	104.18	138.34	0.010
	N-10-0	16	0.0	250.60	399.80	0.111
	N-10	16	5.9	260.99	416.37	0.110
	N-11	16	10.2	228.83	369.53	0.096
	N-12	16	28.7	249.55	409.33	0.099
	N-13	16	33.8	234.70	392.55	0.062
	N-14	16	37.8	241.74	424.23	0.050
	N-15	16	38.5	224.11	357.54	0.109
	N-16-0	19	0.0	413.20	622.90	0.120
	N-16	19	23.2	360.47	535.30	0.074
	N-17	19	35.2	235.93	490.25	0.022
	N-18	19	50.7	243.06	341.14	0.007
	A-0	13	0.0	420.80	641.20	0.127
	A-1	13	8.5	423.10	672.73	0.108
	A-2	13	9.5	423.12	666.00	0.076
	A-3	13	12.0	382.55	619.34	0.080
	A-4	13	13.2	421.77	635.29	0.070
	A-5	13	13.7	409.59	661.26	0.076
	A-6	13	13.8	429.59	654.59	0.053
	A-7	13	14.9	449.97	670.59	0.090
	A-8	13	15.3	417.32	651.04	0.074
	A-9	13	18.6	377.38	622.29	0.069
	A-10	13	21.3	417.06	643.64	0.059

(continued on next page)

(*continued*)

Author	Specimen name	d_{b0} (mm)	Mass loss (%)	f_{yexp} (MPa)	f_{uexp} (MPa)	$e_{u,exp}$
	A-11	13	22.7	408.28	638.71	0.059
	A-12	13	28.4	382.01	626.87	0.056
	A-13	13	31.4	386.45	579.51	0.045
	A-14-0	29	0.0	459.80	658.30	0.127
	A-14	29	4.2	446.36	645.93	0.117
	A-15	29	5.0	464.64	658.30	0.108
	A-16	29	5.7	468.09	656.21	0.091
	A-17	29	5.8	453.94	642.93	0.087
	A-18	29	6.4	451.94	632.98	0.082
	A-19	29	7.3	446.41	660.43	0.084
	A-20	29	8.2	425.74	616.71	0.063
	A-21	29	8.4	446.75	618.05	0.062
	A-22	29	9.4	421.23	624.88	0.089
	A-23	29	10.1	444.97	637.06	0.094
	A-24	29	10.9	397.36	583.68	0.055
	A-25	29	11.4	456.69	653.84	0.075
	A-26	29	12.1	413.24	614.11	0.067
	A-27	29	13.6	409.78	624.78	0.075
	A-28	29	17.1	377.16	563.80	0.056
	A-29	29	19.9	378.86	583.51	0.049
Yu et al. [17]	CB	16	0.0	542.00	631.00	0.210
	6B	16	5.0	505.10	631.38	0.104
	2F	16	6.3	511.10	623.13	0.096
	2B	16	6.5	497.11	590.12	0.095
	5F	16	7.7	465.82	579.57	0.083
Apostolopoulos et al. [11]	B400C-1	16	0.0	435.00	549.23	0.153
	B400C-2	16	5.4	456.46	549.09	0.061
	B400C-3	16	9.3	449.10	543.09	0.047
	B450C-1	16	0.0	536.40	647.95	0.115
	B450C-2	16	6.1	566.09	654.46	0.043
	B450C-3	16	10.9	567.32	644.00	0.027
	B500B-1	16	0.0	523.00	638.35	0.140
	B500B-2	16	5.4	549.14	642.25	0.049
	B500B-3	16	10.8	549.54	636.63	0.030
Moreno et al. [14]	R-01-16	16	0.0	540.91	649.10	–
	R-02-16	16	4.0	517.49	632.38	–
	R-03-16	16	5.0	533.82	636.94	-
	R-04-16	16	5.1	531.02	652.92	-
	R-05-16	16	6.6	562.10	672.61	-
	R-06-16	16	7.4	525.59	645.23	-
	R-07-16	16	7.6	505.78	634.05	-
	R-08-16	16	7.9	530.27	633.08	-
	R-09-16	16	8.0	543.22	642.55	-
	R-10-16	16	8.5	550.09	653.04	-
	R-11-16	16	9.1	528.91	647.80	-
	R-12-16	16	9.2	554.11	658.14	-
	R-13-16	16	10.1	523.62	626.51	-
	R-14-16	16	10.4	474.68	582.36	-
	R-15-16	16	11.4	458.87	578.87	-
	R-16-16	16	11.8	469.31	616.48	-
	R-17-16	16	11.9	495.81	591.00	-
	R-18-16	16	12.3	517.37	617.62	-
	R-19-16	16	12.4	491.92	593.73	-
	R-20-16	16	12.4	512.13	609.23	-
	R-21-16	16	13.0	504.42	594.38	-
	R-22-16	16	13.3	506.71	621.47	-
	R-23-16	16	13.6	527.69	633.20	-
	R-24-16	16	13.7	514.42	620.42	-
	R-25-16	16	15.1	519.29	574.25	-
	R-26-16	16	15.2	521.12	622.61	-
	R-01-20	20	0.0	550.2	666.12	-
	R-02-20	20	5.8	542.01	649.72	-
	R-03-20	20	6.1	505.61	621.47	-
	R-04-20	20	6.7	526.2	637.46	-
	R-05-20	20	7.1	487.32	603.8	-
	R-06-20	20	7.3	561.9	657.81	-
	R-07-20	20	7.5	497.2	613.94	-
	R-08-20	20	7.7	535.71	642.97	-
	R-09-20	20	7.9	545.7	652.73	-
	R-10-20	20	8.0	534.51	643.59	-
	R-11-20	20	8.3	544.2	651.58	-
	R-12-20	20	8.5	459.61	596.1	-
	R-13-20	20	8.6	503.13	610.57	-
	R-14-20	20	9.2	532.72	610.54	-
	R-15-20	20	9.5	505.51	620.93	-
	R-16-20	20	10.3	485.11	612.96	-

(*continued on next page*)

(*continued*)

Author	Specimen name	d_{b0} (mm)	Mass loss (%)	f_{yexp} (MPa)	f_{uexp} (MPa)	$e_{u,exp}$
	R-17-20	20	10.5	518.9	639.54	-
	R-18-20	20	11.2	512.51	601.18	-
	R-19-20	20	11.2	497.41	613.11	-
	R-20-20	20	11.5	542.01	650.86	-
	R-21-20	20	12.1	487.8	631.33	-
	R-22-20	20	12.2	490.32	615.45	-
	R-23-20	20	12.3	482.22	601	-
	R-24-20	20	12.8	473.21	604.09	-
	R-25-20	20	13.2	470.53	594.96	-
	R-26-20	20	13.5	539.11	654.77	-
	R-27-20	20	14.2	485.5	615.11	-
	R-28-20	20	14.3	486.31	625.42	-
	R-29-20	20	14.4	490.9	611.84	-
	R-30-20	20	14.7	512.51	618.23	-
	R-31-20	20	15.1	495.2	613.32	-
	R-32-20	20	17.4	479.91	608.79	-
Zhang et al. [16]	At1	6.5	0.0	261.3	422.9	-
	At2	6.5	17.1	250.5	387.4	-
	At3	6.5	29.4	236.8	367.4	-
	At4	6.5	17.6	237.3	362.2	-
	At5	6.5	22.7	244.1	378.2	-
	At6	6.5	23.7	268.1	369.4	-
	At7	6.5	22.2	246.5	376.8	-
	At8	6.5	28.6	242.4	350.0	-
	At9	6.5	28.5	232.3	348.2	-
	At10	6.5	25.7	232.7	399.2	-
	At11	6.5	16.2	231.7	389.6	-
	At12	6.5	17.4	242.5	392.9	-
	At13	6.5	20.2	245.2	383.4	-
	At14	6.5	23.5	224.7	352.3	-
	At15	6.5	15.6	246.2	388.6	-
	At16	6.5	23.5	261.5	396.2	-
	At17	6.5	18.9	256.3	411.0	-
	At18	6.5	16.0	274.1	404.1	-
	At19	6.5	18.5	282.4	390.2	-
	At20	6.5	16.6	284.5	422.8	-
	At21	6.5	22.5	276.7	382.3	-
	At22	6.5	19.6	250.9	384.4	-
	At23	6.5	18.0	266.5	390.4	-
	At24	6.5	19.2	263.4	389.1	-
	At25	6.5	20.3	256.0	370.6	-
	At26	6.5	19.5	302.7	361.5	-
	At27	6.5	20.2	274.8	409.3	-
	At28	6.5	17.6	284.5	409.4	-
	At29	6.5	29.7	244.5	378.0	-
	At30	6.5	25.5	237.1	364.2	-
	At31	6.5	21.0	239.6	378.9	-
	At32	6.5	18.3	244.2	370.8	-
	At33	6.5	21.8	235.0	383.0	-
	At34	6.5	19.0	251.5	391.8	-
	At35	6.5	26.5	220.9	319.0	-
	At36	6.5	16.4	279.1	398.9	-
	At37	6.5	20.7	277.8	349.4	-
	At38	6.5	17.2	269.7	400.7	-
	At39	6.5	17.1	264.5	400.4	-
	At40	6.5	18.7	254.2	348.2	-
	At41	6.5	22.7	223.3	364.0	-
	At42	6.5	31.2	240.7	359.8	-
	At43	6.5	25.5	258.5	383.4	-
	At44	6.5	27.2	261.2	374.0	-
	At45	6.5	20.4	253.1	361.3	-
	Bt1	12	0.0	370.8	549.7	-
	Bt2	12	10.0	387.7	561.5	-
	Bt3	12	6.1	380.7	587.7	-
	Bt4	12	6.0	375.8	488.3	-
	Bt5	12	4.5	354.7	506.8	-
	Bt6	12	12.3	347.8	476.5	-
	Bt7	12	12.3	340.3	456.4	-
	Bt8	12	9.1	380.9	547.2	-
	Bt9	12	11.9	383.8	539.5	-
	Bt10	12	39.7	350.7	374.1	-
	Bt11	12	20.5	348.0	552.7	-
	Bt12	12	9.7	340.2	539.1	-
	Bt13	12	9.3	363.1	567.3	-
	Bt14	12	17.0	364.0	578.5	-
	Bt15	12	18.3	364.7	564.8	-

(*continued on next page*)

(*continued*)

Author	Specimen name	d_{b0} (mm)	Mass loss (%)	f_{yexp} (MPa)	f_{uexp} (MPa)	$e_{u,exp}$
	Bt16	12	27.2	375.9	564.5	-
	Bt17	12	25.6	358.9	559.1	-
	Bt18	12	24.0	360.9	556.5	-
	Bt19	12	35.8	329.4	494.6	-
	Bt20	12	35.6	352.8	531.3	-
	Bt21	12	32.3	370.5	533.3	-

Dataset 2 – Monotonic pullout tests on corroded bars.

Author	Specimen	d_b(mm)	c/d_b	f'_c(MPa)	mass loss (%)	$u_{b,corr}$(MPa)
Yalciner et al. [24]	R4SP1	14	1.07	40.8	8.9	3.7
	R4SP2	14	1.07	40.8	4.1	13
	R4SP3	14	1.07	40.8	2.47	11.2
	R4SP4	14	1.07	40.8	2.72	11.7
	R4SP5	14	1.07	40.8	4.32	12.2
	R4SP6	14	1.07	40.8	4.33	12.2
	R4SP7	14	1.07	40.8	4.09	13
	R4SP8	14	1.07	40.8	6.51	3.2
	R4SP9	14	1.07	40.8	14.52	2.1
	R5SP1	14	2.14	40.8	1.37	18
	R5SP2	14	2.14	40.8	3.45	9.6
	R5SP3	14	2.14	40.8	5.56	3.3
	R5SP4	14	2.14	40.8	1.4	17.9
	R5SP5	14	2.14	40.8	1.69	16.9
	R5SP6	14	2.14	40.8	1.6	17
	R5SP7	14	2.14	40.8	3.57	8.9
	R5SP8	14	2.14	40.8	5.36	3.7
	R5SP9	14	2.14	40.8	16.65	2.1
	R6SP1	14	3.21	40.8	0.69	19.1
	R6SP2	14	3.21	40.8	1.69	13.4
	R6SP3	14	3.21	40.8	2.66	12.4
	R6SP4	14	3.21	40.8	0.68	17.9
	R6SP5	14	3.21	40.8	0.66	18.9
	R6SP6	14	3.21	40.8	0.84	18.3
	R6SP7	14	3.21	40.8	0.88	18.2
	R6SP8	14	3.21	40.8	1.6	13.7
	R6SP9	14	3.21	40.8	3.81	1.3
	R7SP1	14	1.07	40.8	18.75	4.3
	R7SP2	14	1.07	40.8	8.9	3
	R7SP3	14	1.07	40.8	14.66	2
	R8SP1	14	2.14	40.8	6.87	6.5
	R8SP2	14	2.14	40.8	17.33	1.8
	R8SP3	14	2.14	40.8	6.4	5.5
	R9SP1	14	3.21	40.8	6.27	3.2
	R9SP2	14	3.21	40.8	0.68	18
	R9SP3	14	3.21	40.8	3.81	1.3
	R13SP1	14	1.07	18.4	1.33	18.5
	R13SP2	14	1.07	18.4	7.48	3.5
	R13SP3	14	1.07	18.4	4.47	6.3
	R13SP4	14	1.07	18.4	0.77	22.3
	R13SP5	14	1.07	18.4	0.8	22.4
	R13SP6	14	1.07	18.4	0.9	21.7
	R13SP7	14	1.07	18.4	0.94	21.5
	R13SP8	14	1.07	18.4	7.56	3.5
	R13SP9	14	1.07	18.4	3.3	7.5
	R14SP1	14	2.14	18.4	0	20.4
	R14SP2	14	2.14	18.4	5.14	6.2
	R14SP3	14	2.14	18.4	5.46	2.4
	R14SP4	14	2.14	18.4	0.65	23.8
	R14SP5	14	2.14	18.4	0.68	3.9
	R14SP6	14	2.14	18.4	0.77	23.5
	R14SP7	14	2.14	18.4	0.77	23.4
	R14SP8	14	2.14	18.4	1.7	14
	R14SP9	14	2.14	18.4	4.45	4.2
	R15SP1	14	3.21	18.4	0	28.3
	R15SP2	14	3.21	18.4	2.69	7.6
	R15SP3	14	3.21	18.4	0.34	26.2
	R15SP4	14	3.21	18.4	0.31	31.6
	R15SP5	14	3.21	18.4	0.4	31
	R15SP6	14	3.21	18.4	0.41	30.8
	R15SP7	14	3.21	18.4	4.73	3
	R15SP8	14	3.21	18.4	4.38	3.4
	R15SP9	14	3.21	18.4	4.17	3.9
	R16SP1	14	1.07	18.4	8.95	3
	R16SP2	14	1.07	18.4	6.9	8

(*continued on next page*)

(*continued*)

Author	Specimen	d_b(mm)	c/d_b	f'_c(MPa)	mass loss (%)	$u_{b,corr}$(MPa)
	R16SP3	14	1.07	18.4	3.41	6.8
	R17SP1	14	2.14	18.4	9.9	5.9
	R17SP2	14	2.14	18.4	4.86	1.7
	R17SP3	14	2.14	18.4	1.72	13.8
	R18SP1	14	3.21	18.4	0.34	26.9
	R18SP2	14	3.21	18.4	0.34	31.7
	R18SP3	14	3.21	18.4	3.08	6.1
Lee et al. [23]	1a	13	4.04	24.7	3.2	4
	2a	13	4.04	24.7	16.8	1.5
Chung et al. [22]	A13-2-0.1	13	5.77	28.3	0.1	20
	A13-2-0.5	13	5.77	28.3	0.5	17
	A13-2-1.0	13	5.77	28.3	1	20
	A13-3-1.1a	13	5.77	28.3	1.1	14
	A13-3-1.2	13	5.77	28.3	1.2	16.2
	A13-3-1.4	13	5.77	28.3	1.4	18
	A13-4-0.9	13	5.77	28.3	0.9	16.4
	A13-4-2.5a	13	5.77	28.3	2.5	20.6
	A13-4-0.2a	13	5.77	28.3	0.2	16
	A13-5-0.8	13	5.77	28.3	0.8	18.5
	A13-5-1.9	13	5.77	28.3	1.9	20.3
	A13-5-0.9a	13	5.77	28.3	0.9	14.1
	A13-7-0.5a	13	5.77	28.3	0.5	16.7
	A13-7-1.4a	13	5.77	28.3	1.4	19
	A13-7-2.2	13	5.77	28.3	2.2	14.4
	A13-10-0.6a	13	5.77	28.3	0.6	16.1
	A13-10-0.7a	13	5.77	28.3	0.7	15.4
	A13-10-1.9	13	5.77	28.3	1.9	15.9
Cabrera [21]	2	12	6.25	40	0.71	23.5
	3	12	6.25	40	2.42	19
	4	12	6.25	40	6.9	13.5
	5	12	6.25	40	8.3	12.5
	6	12	6.25	40	12	8.5
Auyeung et al. [66]	3	19	4.68	28	0.72	7.66
	4	19	4.68	28	0.72	6.96579
	5	19	4.68	28	0.98	8.13709
	6	19	4.68	28	1.23	4.91
	7	19	4.68	28	1.44	3.445
	8	19	4.68	28	1.7	4.24424
	9	19	4.68	28	2.2	3.54146
	10	19	4.68	28	2.88	1.9981
	11	19	4.68	28	5.2	1.46068
Al-sulaimani et al. [67]	10_1	10	7.50	30	0.3	20.4
	10_2	10	7.50	30	0.5	21.9
	10_3	10	7.50	30	0.87	23.9
	10_4	10	7.50	30	1.5	22.3
	10_5	10	7.50	30	1.83	21.2
	10_6	10	7.50	30	2.66	19.1
	10_7	10	7.50	30	3.25	17.7
	10_8	10	7.50	30	4.27	14.5
	10_9	10	7.50	30	4.52	14.4
	10_10	10	7.50	30	4.81	10.9
	10_11	10	7.50	30	6.67	9.7
	10_12	10	7.50	30	6.7	7.1
	10_13	10	7.50	30	8.75	3.1
	10_14	10	7.50	30	7.15	3.7
	10_15	10	7.50	30	7.8	2.6
	14_1	14	5.36	30	0.3	19.1
	14_2	14	5.36	30	0.76	21
	14_3	14	5.36	30	0.9	21.1
	14_4	14	5.36	30	1.22	19
	14_5	14	5.36	30	1.36	20.4
	14_6	14	5.36	30	1.62	18.7
	14_7	14	5.36	30	2.75	15.5
	14_8	14	5.36	30	2.89	16
	14_9	14	5.36	30	3	14.6
	14_10	14	5.36	30	3.33	13.2
	14_11	14	5.36	30	3.33	13.4
	14_12	14	5.36	30	4.29	10.7
	14_13	14	5.36	30	5.15	7.9
	14_14	14	5.36	30	5.45	4.8
	14_15	14	5.36	30	6.5	4.1
	20_1	20	3.75	30	0.3	19.1
	20_2	20	3.75	30	0.5	19.4
	20_3	20	3.75	30	0.65	19.7
	20_4	20	3.75	30	0.78	18.3
	20_5	20	3.75	30	1.16	17.6

(*continued on next page*)

(*continued*)

Author	Specimen	d_b(mm)	c/d_b	f'_c(MPa)	mass loss (%)	$u_{b,corr}$(MPa)
	20_6	20	3.75	30	1.67	13.7
	20_7	20	3.75	30	1.86	15.7
	20_8	20	3.75	30	2	14.4
	20_9	20	3.75	30	2.69	11.8
	20_10	20	3.75	30	2.87	11.4
	20_11	20	3.75	30	3.08	11.6
	20_12	20	3.75	30	3.13	11.7
	20_13	20	3.75	30	3.6	9.6
	20_14	20	3.75	30	4.25	8
	20_15	20	3.75	30	4.35	8
Almusallam et al. [19]	1	12	5.81	40	3.6	17.7
	2	12	5.81	40	4	18.2
	3	12	5.81	40	4.78	16.1
	4	12	5.81	40	5.09	13.5
	5	12	5.81	40	7	4.7
	6	12	5.81	40	15.65	3.054287
	7	12	5.81	40	20.5	2.86
	8	12	5.81	40	32.5	2.8
	9	12	5.81	40	48.25	2.34
	10	12	5.81	40	60	2.2
	11	12	5.81	40	80	1.82
Jin and Zhao [18]	D1	12	4.17	17.7	0.12	8.92
	D2	12	4.17	17.7	0.16	9.48
	D3	12	4.17	17.7	0.24	7.36
	D4	12	4.17	17.7	0.32	8.45
	D5	12	4.17	17.7	0.43	8.39
	D6	12	4.17	17.7	0.62	10.61
	D7	12	4.17	17.7	0.81	11.34
	D8	12	4.17	17.7	1.66	9.72
	D9	12	4.17	17.7	4.64	7.5
	D10	12	4.17	17.7	5.97	5.68
	D11	12	4.17	17.7	8.7	4.45
	D12	12	4.17	17.7	8.6	3.75
	D13	12	4.17	17.7	9.95	2.54
	D14	12	4.17	17.7	9.99	1.4
Soudki and Sherwood [25]	15-U-1	10	2.00	35	1	6.5
	15-U-5	10	2.00	35	5	11
	15-U-10	10	2.00	35	10	6.32
	30-U-1	10	3.50	35	1	13.8
	30-U-3	10	3.50	35	3	12.5
	30-U-5	10	3.50	35	5	13.65
	30-U-7	10	3.50	35	7	10.3
	30-U-10	10	3.50	35	10	4.775
	60-U-1	10	6.50	35	1	14.43
	60-U-3	10	6.50	35	3	14.4
	60-U-5	10	6.50	35	5	14.2
	60-U-7	10	6.50	35	7	13.47
	60-U-10	10	6.50	35	10	9.1

Dataset 3 – Flexure-controlled singly reinforced beams with corroded tensile reinforcement under monotonic point loading.

Author	Specimen	b(mm)	D(mm)	a/d	d_b(mm)	f_y(MPa)	f'_c(MPa)	m_{loss}(%)	V_{exp}(kN)
Torres-costa et al. [27]	B03	100	150	5.6	9.5	570	27	9.5	7.5
	B04	100	150	5.6	9.5	570	27	16.5	4.3
	B05	100	150	5.6	9.5	570	27	17.2	4.5
	B06	100	150	5.6	9.5	570	27	11.2	7.9
	B07	100	150	5.6	9.5	570	27	10.1	7.5
	B08	100	150	5.6	9.5	570	27	19.7	7.1
	B09	100	150	5.6	9.5	570	27	18	6.5
	B10	100	150	5.6	9.5	570	27	29.8	3.1
Mangat and Elgarf [26]	8_1.25_1	100	150	2.31	10	520	40	2.5	62.4
	8_2.5_1	100	150	2.31	10	520	40	5	58.2
	8_3.75_1	100	150	2.31	10	520	40	7.4	53.0
	8_5_1	100	150	2.31	10	520	40	9.75	49.4
	8_7.5_1	100	150	2.31	10	520	40	14.4	39
	8_10_1	100	150	2.31	10	520	40	19	27.63
	8_1.25_2	100	150	2.31	10	520	40	2.5	60.5
	8_2.5_2	100	150	2.31	10	520	40	5	57
	8_3.75_2	100	150	2.31	10	520	40	7.4	51
	8_5_2	100	150	2.31	10	520	40	9.75	46
	8_7.5_2	100	150	2.31	10	520	40	14.4	32
	8_10_2	100	150	2.31	10	520	40	19	25
	8_1.25_4	100	150	2.31	10	520	40	2.5	60
	8_2.5_4	100	150	2.31	10	520	40	5	55
	8_3.75_4	100	150	2.31	10	520	40	7.4	49

(*continued on next page*)

(*continued*)

Author	Specimen	b(mm)	D(mm)	a/d	d_b(mm)	f_y(MPa)	f'_c(MPa)	m_{loss}(%)	V_{exp}(kN)
	8_5_4	100	150	2.31	10	520	40	9.75	40
	8_7.5_4	100	150	2.31	10	520	40	14.4	28
	8_10_4	100	150	2.31	10	520	40	19	15
	6_1.25_3	100	150	2.31	10	520	40	2.5	61.4
	6_2.5_3	100	150	2.31	10	520	40	5	57.9
	6_3.75_3	100	150	2.31	10	520	40	7.4	51.0
	6_5_3	100	150	2.31	10	520	40	9.75	43.9
	6_7.5_3	100	150	2.31	10	520	40	14.4	30.6
	6_10_3	100	150	2.31	10	520	40	19	15.9
	7_2.5_2	100	150	2.31	8	520	40	5	38.9
	7_5_2	100	150	2.31	8	520	40	9.75	31.2
	7_7.5_2	100	150	2.31	8	520	40	14.4	22.6
	7_10_2	100	150	2.31	8	520	40	19	16.8

Dataset 4 – Shear-controlled beams with corroded stirrups under monotonic loading.

Author	Specimen	b (mm)	D (mm)	a/d	Longitudinal reinforcement		Stirrups		V_{exp} (kN)
					m_{loss} (%)	ρ_l (%)	m_{loss} (%)	ρ_t (%)	
El-sayed et al. [28]	B10-200	200	350	2.91	0	3.43	7.2	0.25	157
	B20-200	200	350	2.91	0	3.43	17	0.25	136
	B10-150	200	350	2.91	0	3.43	10.3	0.34	166
	B20-150	200	350	2.91	0	3.43	16.3	0.34	173
	B10-100	200	350	2.91	0	3.43	9	0.50	204
	B20-100	200	350	2.91	0	3.43	18	0.50	172.5
Li et al. [29]	B1	120	200	2.35	0	2.77	1.6	0.24	61.2
	B2	120	200	2.35	0	2.77	3.4	0.24	58.15
	B3	120	200	2.35	0	2.77	5.1	0.24	45
	B4	120	200	2.35	0	2.77	6	0.24	55
	B5	120	200	2.35	0	2.77	6.7	0.24	42.5
	B6	120	200	2.35	0	2.77	7	0.24	52
	B7	120	200	2.35	0	2.77	8.9	0.24	40
Yu et al. [31]	Bs04-B	150	280	1.94	0	0.73	22.8	0.17	72.5
	Bs04-A	150	280	1.94	0	0.73	26.6	0.17	65
	Bs02-B	150	280	1.55	0	0.73	9.2	0.17	100
	Bs02-A	150	280	2.03	0	0.73	8.8	0.17	65
Xia et al. [30]	A-1	120	230	1.63	0	3.56	10.7	0.47	63.2
	A-2	120	230	1.63	0	3.56	27	0.47	56
	A-3	120	230	1.63	0	3.56	37	0.47	56.25
	A-4	120	230	1.63	0	3.56	42.5	0.47	52.7
	A-5	120	230	1.63	0	3.56	54	0.47	42.6
	B-1	120	230	1.63	0	3.56	12.9	0.47	62
	B-2	120	230	1.63	0	3.56	21.75	0.47	61.65
	B-3	120	230	1.63	0	3.56	29.2	0.47	62
	B-4	120	230	1.63	0	3.56	41.5	0.47	59.5
	B-5	120	230	1.63	0	3.56	51.4	0.47	50
	C-1	120	230	1.63	0	3.56	6.53	0.56	67
	C-2	120	230	1.63	0	3.56	11.73	0.56	64.5
	C-3	120	230	1.63	0	3.56	19.5	0.56	64.05
	C-4	120	230	1.63	0	3.56	25.7	0.56	65.75
	C-5	120	230	1.63	0	3.56	32.4	0.56	63.5
Higgins and Farrow [32]	8RA	254	610	2.15	0	2.55	0	0.52	594
	8RD	254	610	2.15	0	2.55	28.9	0.52	471
	10RA	254	610	2.15	0	2.55	0	0.42	578
	10RB	254	610	2.15	0	2.55	13.2	0.42	507
	10RC	254	610	2.15	0	2.55	23.1	0.42	467
	10RD	254	610	2.15	0	2.55	26	0.42	405
	12RA	254	610	2.15	0	2.55	0	0.35	489
	12RD	254	610	2.15	0	2.55	33.8	0.35	443
Juarez et al. [34]	V71-150	200	350	2.07	0	1.73	0	0.34	115
	V81-150	200	350	2.07	0	1.73	0	0.34	120
	V3M-150	200	350	2.07	0	1.73	26.85	0.34	68
	V4M-150	200	350	2.07	0	1.73	47.63	0.34	91
	V5S-150	200	350	2.07	0	1.73	64.94	0.34	80
	V6S-150	200	350	2.07	0	1.73	56.72	0.34	86
	V131-200	200	350	2.07	0	1.73	0	0.25	120
	V141-200	200	350	2.07	0	1.73	0	0.25	98
	V11M-200	200	350	2.07	0	1.73	37.67	0.25	77
	V12M-200	200	350	2.07	0	1.73	26.85	0.25	87
	V15S-200	200	350	2.07	0	1.73	64.94	0.25	80
	V16S-200	200	350	2.07	0	1.73	64.94	0.25	89
Imam and Azad [33]	A1-10	140	220	1.76	0	3.06	28.55	0.90	96.1
	A2-10	140	220	1.76	0	3.06	30.19	0.90	81.6
	A3-10	140	220	1.76	0	3.06	38.72	0.90	83.5
	A4-6	140	220	1.76	0	3.06	20.93	0.90	88.5

(*continued on next page*)

(*continued*)

Author	Specimen	b (mm)	D (mm)	a/d	Longitudinal reinforcement		Stirrups		V_{exp} (kN)
					m_{loss} (%)	ρ_l (%)	m_{loss} (%)	ρ_t (%)	
	A5-6	140	220	1.76	0	3.06	22.39	0.90	87.6
	A6-6	140	220	1.76	0	3.06	19.39	0.90	90
	A7-6	140	220	1.76	0	3.06	21.03	0.90	103
	B1-10	150	240	1.76	0	2.86	29.42	0.84	80.9
	B2-10	150	240	1.76	0	2.86	26.79	0.84	103
	B3-10	150	240	1.76	0	2.86	22.98	0.84	105
	B4-10	150	240	1.76	0	2.86	29.11	0.84	90
	B5-6	150	240	1.76	0	2.86	16.79	0.84	119.1
	B6-6	150	240	1.76	0	2.86	16.79	0.84	110
Rodriguez et al. [10]	123	150	200	4.71	12.3	2.17	78.2	0.39	37.3
	124	150	200	4.71	15.4	2.17	86.6	0.39	27.9
	125	150	200	4.71	15.1	2.17	93.8	0.39	31.4
	136	150	200	4.71	13.5	2.17	86.6	0.39	29.1
	135	150	200	4.71	13.8	2.17	93.8	0.39	33.9
	215	150	200	4.71	10.7	2.56	66	0.39	38.6
	216	150	200	4.71	11.6	2.56	82.6	0.39	36.2
	213	150	200	4.71	14.1	2.56	86.6	0.39	26.6
	214	150	200	4.71	15.4	2.56	97.2	0.39	28.7
	315	150	200	4.71	16.9	2.56	97.2	0.79	27.7
Lu et al. [35]	A-1	200	300	2.00	14.4	2.51	54.2	0.19	147.7
	A-2	200	300	2.50	1.8	2.51	7.6	0.14	137.8
	A-3	200	300	3.00	16.5	2.51	46.5	0.20	119.8
	A-4	200	300	3.50	15.6	2.51	44.3	0.25	109.8
	A-5	200	300	2.00	15.5	2.51	55.6	0.19	151.6
	A-6	200	300	2.50	0	2.51	0	0.14	139.2
	A-7	200	300	3.00	22.7	2.51	60.1	0.20	115.4
	A-9	200	300	2.00	9.9	2.51	38.2	0.19	181.5
	A-10	200	300	2.50	4.3	2.51	17.6	0.14	111.8
	A-11	200	300	3.00	12.7	2.51	38.7	0.20	93.8
	A-12	200	300	3.50	13.5	2.51	40.8	0.25	121.3
	B-1	200	300	2.00	0	2.51	0	0.19	145.4
	B-2	200	300	2.50	3.2	2.51	13.3	0.14	119.8
	B-3	200	300	3.00	10.4	2.51	30.5	0.20	125.7
	B-5	200	300	2.00	10.4	2.51	39.4	0.19	179.6
	B-6	200	300	2.50	14.1	2.51	51.4	0.14	133.5
	B-7	200	300	3.00	15.8	2.51	44.1	0.20	115.8
	B-9	200	300	2.00	13.7	2.51	51.1	0.19	129.2
	B-10	200	300	2.50	10.6	2.51	40.7	0.14	155.8
	B-11	200	300	3.00	10.5	2.51	32.4	0.20	109.8
Xue et al. [36]	B(39)-s0	120	240	2.64	0	2.20	0	0.39	74
	B(39)-s1	120	240	2.64	0.8	2.20	6.1	0.39	72
	B(39)-s2	120	240	2.64	1	2.20	8.3	0.39	74
	B(39)-s3	120	240	2.64	1.6	2.20	14	0.39	69.5
	B(39)-s4	120	240	2.64	1.8	2.20	16.3	0.39	70.4
	B(39)-s5	120	240	2.64	0.9	2.20	19.3	0.39	69.5
	B(52)-s0	120	240	2.64	0	2.20	0	0.52	84
	B(52)-s1	120	240	2.64	0.8	2.20	5.5	0.52	87.9
	B(52)-s2	120	240	2.64	0.7	2.20	9.1	0.52	80.7
	B(52)-s3	120	240	2.64	0.7	2.20	13.4	0.52	72.1
Zhao and Jin [37]	1–0	150	180	3.00	0	3.04	0	0.30	40
	1–1	150	180	3.00	0	3.04	0.6	0.30	40
	1–2	150	180	3.00	0	3.04	1.8	0.30	40
	1–3	150	180	3.00	0	3.04	2.4	0.30	48
	1–4	150	180	3.00	0	3.04	3.3	0.30	50
	1–5	150	180	3.00	0	3.04	4	0.30	46
	2–0	150	180	3.00	0	3.04	0	0.44	48
	2–1	150	180	3.00	0	3.04	0.4	0.44	42
	2–2	150	180	3.00	0	3.04	0.7	0.44	40
	2–3	150	180	3.00	0	3.04	2.2	0.44	44
	2–4	150	180	3.00	0	3.04	3.5	0.44	42
	2–5	150	180	3.00	0	3.04	4.9	0.44	52
	3–0	150	180	3.00	0	3.04	0	0.30	36
	3–1	150	180	3.00	0	3.04	0.8	0.30	38
	3–2	150	180	3.00	0	3.04	2	0.30	48
	3–3	150	180	3.00	0	3.04	3.8	0.30	40
	3–4	150	180	3.00	0	3.04	3.8	0.30	46
	3–5	150	180	3.00	0	3.04	3.7	0.30	46
	0	150	180	2.20	0	2.71	0	0.22	60
	1	150	180	2.20	1.5	2.71	0.8	0.22	60
	2	150	180	2.20	2.8	2.71	1.7	0.22	65
	3	150	180	2.20	4.2	2.71	2.7	0.22	68
	4	150	180	2.20	6.6	2.71	4	0.22	69
	5	150	180	2.20	8.6	2.71	5.1	0.22	68
	6	150	180	2.20	11.6	2.71	6.3	0.22	72

(*continued on next page*)

(*continued*)

Author	Specimen	b (mm)	D (mm)	*a/d*	Longitudinal reinforcement		Stirrups		V_{exp} (kN)
					m_{loss} (%)	ρ_l (%)	m_{loss} (%)	ρ_t (%)	
	7	150	180	2.20	14	2.71	7.2	0.22	70
	8	150	180	2.20	19	2.71	8.3	0.22	67
	9	150	180	2.20	26	2.71	9.2	0.22	62

Dataset 5 – Cyclic tests on corroded beam-column components.

Author	Specimen	*b* (mm)	*D* (mm)	*a/d*	M_l (%)	*Mt* (%)	*s/d*	$P/A_g f'_c$	V_{max} (kN)	θ_u (%)
Ou et al. [8]	B12.5	300	500	3.5	1.38	1.7	0.23	0	158	4.8
	B25	300	500	3.5	1.8	3.08	0.23	0	149	4.7
	B50	300	500	3.5	2.19	4.08	0.23	0	148	4.4
	B150	300	500	3.5	3.37	8.03	0.23	0	120	2.6
Ou and Chen [48]	Bt-3	300	500	2.8	0	2.9	0.23	0	354.6	4.7
	Bt-6	300	500	2.8	0	5.87	0.23	0	333.4	4.3
	Bt-11	300	500	2.8	0	11.7	0.23	0	340.5	2.9
	Bt-12	300	500	2.8	0	12.4	0.23	0	336.9	2.7
	Bt-16	300	500	2.8	0	15.7	0.23	0	331.7	2.4
	Bt-35	300	500	2.8	0	35.1	0.23	0	319	1.5
Ou and Nguyen [47]	TB-6	300	500	2.8	5.16	6.54	0.23	0	292	4.0
	TB-8	300	500	2.8	8.62	4.16	0.23	0	282	4.3
	TB-13	300	500	2.8	13.82	10.9	0.23	0	240	3.4
	TB-19	300	500	2.8	21.11	7.25	0.23	0	218	2.0
	TB-32	300	500	2.8	29.35	11.3	0.23	0	217	1.7
	TBH-4	300	500	2.8	5.02	15.7	0.23	0	292	3.4
	TBH-6	300	500	2.8	5.37	16.4	0.23	0	289	4.2
	B-3	300	500	2.8	3.26	1.45	0.23	0	258	4.3
	B-9	300	500	2.8	8.74	0.95	0.23	0	260	3.9
	B-13	300	500	2.8	12.94	1.05	0.23	0	248	4.6
	B-16	300	500	2.8	15.75	1.76	0.23	0	209	2.8
	B-33	300	500	2.8	32.92	2.62	0.23	0	200	1.5
	TBt-15	300	500	2.8	16.56	1.56	0.23	0	269	2.7
Vu and Li [7]	C1	350	350	2.9	3.4	11.5	0.16	0.1	238.8	5.1
	C2	350	350	2.9	6.1	14.4	0.16	0.1	193.2	4.7
	C3	350	350	2.9	10.9	25	0.16	0.1	190.7	3.5
	C4	350	350	2.9	3.4	13.6	0.16	0.25	254.4	3.2
	C5	350	350	2.9	3.9	15.5	0.16	0.25	237.1	2.7
	C6	350	350	2.9	7.3	23.5	0.16	0.25	250	2.5
Vu and Li [6]	CC1	350	350	1.8	3.4	11.4	0.16	0.1	359	3.8
	CC2	350	350	1.8	5.8	21.3	0.16	0.1	327.8	3.1
	CC3	350	350	1.8	6.8	26.1	0.16	0.1	293.8	2.7
	CC4	350	350	1.8	3.4	8.4	0.16	0.25	426.6	2.9
	CC5	350	350	1.8	3.3	12.1	0.16	0.25	369	2.8
	CC6	350	350	1.8	7.5	18.2	0.16	0.25	397.5	1.8
Ma et al. [49]	C9–15	260	260	3.8	9.5	0	0.47	0.15	59.15	3.7
	C4–25	260	260	3.8	4.1	0	0.47	0.25	69.23	4.5
	C9–25	260	260	3.8	9.7	0	0.47	0.25	62.5	3.2
	C9–40	260	260	3.8	9.3	0	0.47	0.4	62.1	2.5
	C14–32	260	260	3.8	14.7	0	0.47	0.32	67.6	2.5
	C11–60	260	260	3.8	11.3	0	0.47	0.6	69.5	3.1
Yuan et al., [50]	C5-L0	300	300	4.3	3.83	0	0.30	0	67.38	3.2
	C5-L40	300	300	4.3	3.99	0	0.30	0.4	66.3	2.7
	C5-L60	300	300	4.3	4.45	0	0.30	0.6	70.4	3.2
	C10-L0	300	300	4.3	8	0	0.30	0	64.4	2.7
	C10-L40	300	300	4.3	8.41	0	0.30	0.4	64.45	3.2
	C10-L60	300	300	4.3	7.96	0	0.30	0.6	65.56	2.3
	CG10	300	300	4.3	7.16	18.6	0.30	0	62.2	3.2
Li et al. [9]	RC-2	200	200	4.2	0	4.76	0.42	0.125	73.76	5.5
	RC-3	200	200	4.2	0	12.9	0.42	0.125	66	5.2
	RC-4	200	200	4.2	0	22.2	0.42	0.125	65.15	4.6
	RC-5	200	200	4.2	0	9.23	0.42	0.125	65.56	4.6
	RC-6	200	200	4.2	0	14	0.42	0.125	55.16	4.0
	RC-7	200	200	4.2	0	15.6	0.73	0.125	65.7	4.5
	RC-8	200	200	4.2	0	16.7	0.73	0.125	80	4.2
Li et al. [51]	N1C10	300	300	5.3	6.6	0	0.39	0.13	75	2.5
	N1C20	300	300	5.3	18.5	0	0.39	0.13	60	2.0
	N3C10	300	300	5.3	7.2	0	0.39	0.38	90	2.2
	N3C20	300	300	5.3	17.7	0	0.39	0.38	85	2.0
Yang et al. [52]	ZZ2	210	210	4.9	5.1	6.5	0.49	0.18	60	3.6
	ZZ3	210	210	4.9	8.3	14.8	0.49	0.18	60	3.8
	ZZ4	210	210	4.9	13.25	7.7	0.49	0.18	60	3.5
	ZZ4	210	210	4.9	16.8	9	0.49	0.18	47	3.3
Li et al. [38]	CC-ED0-VA	250	250	5.9	9.9	12.6	0.28	0.25	46.85	3.2
Zheng et al. [39]	SC2	200	200	2.8	2.53	5.32	0.34	0.3	138.4	3.2
	SC3	200	200	2.8	4.54	8.13	0.34	0.3	132	2.8

(*continued on next page*)

(*continued*)

Author	Specimen	*b* (mm)	*D* (mm)	*a/d*	M_l (%)	*Mt* (%)	*s/d*	$P/A_g f'_c$	V_{max} (kN)	θ_u (%)
	SC4	200	200	2.8	6.75	11.5	0.34	0.3	112	2.7
	SC5	200	200	2.8	5.86	12.8	0.45	0.3	105.6	2.6
	SC6	200	200	2.8	6.23	13.2	0.57	0.3	100.8	1.6
Zheng et al. [39]	C1	200	200	5.7	3.73	5.62	0.34	0.2	48	6.0
	C2	200	200	5.7	3.81	5.68	0.34	0.4	57	3.0
	C3	200	200	5.7	3.58	5.66	0.34	0.6	54	2.1
	C5	200	200	5.7	2.44	4.21	0.34	0.4	61.4	3.8
	C6	200	200	5.7	6.2	9.6	0.34	0.4	52.5	2.8
Meda et al. [41]	CC	300	300	5.8	21.5	0	1.15	0.28	46	2.0
Guo et al. [42]	Sp 2	600	250	11	5	11.2	0.44	0.08	58	3.5
	Sp 3	600	250	11	9.74	19.8	0.44	0.08	53	3.0
	Sp 4	600	250	11	15.2	30.2	0.44	0.08	53	1.7
Dai et al. [43]	C-A-0.1	300	300	3.8	1.87	1.65	0.30	0.09	136	4.4
	C-E-0.1	300	300	3.8	2.07	7.43	0.30	0.09	126	3.8
	C-A-0.45	300	300	3.8	2.33	2.52	0.30	0.45	190	2.6
	C-E-0.45	300	300	3.8	2.16	6.8	0.30	0.45	186	2.0
Karimipour and Edalati [44]	WF5	250	250	4.8	2.7	6.5	0.39	0.10	73	4.0
	WF10	250	250	4.8	5.4	8	0.39	0.10	73	4.0
	WF15	250	250	4.8	6.9	10	0.39	0.10	70	3.6
	WF20	250	250	4.8	9.5	15.5	0.39	0.10	60	3.5
Rajput and Sharma [45]	UC15%	300	300	6.0	15.56	15.8	1.19	0.35	69	2.7
	UC30%	300	300	6.0	30.16	22.6	1.19	0.32	67.6	2.0
Funaki et al. [46]	C07C-N3	400	400	2.3	0.6	0.9	0.17	0.2	410	3.0
	C09C-N5	400	400	2.3	1	1.7	0.17	0.2	413	2.5
	C10C-N6	400	400	2.3	1.5	1.9	0.17	0.2	368	2.0
	C07C-F3	400	400	2.3	0.8	0.5	0.17	0.2	418	3.0
	C09C-F5	400	400	2.3	0.5	1	0.17	0.2	431	3.0
	C10C-F6	400	400	2.3	0.5	1.1	0.17	0.2	403	3.0
	C07C-L3	400	400	2.3	1.6	3.6	0.17	0.2	333	3.0
	C07C-L5	400	400	2.3	3.7	5.3	0.17	0.2	346	3.0
	C07C-L6	400	400	2.3	5.3	6.2	0.17	0.2	300	2.5
Goksu and Ilki [13]	NSX9	200	300	4	9	0	0.4	0.19	59.1	8.0
	NSX13	200	300	4	13	0	0.4	0.19	45	6.0
	NSX16	200	300	4	16	0	0.4	0.19	50.9	4.6
	NSX22	200	300	4	22	0	0.4	0.19	51.9	4.0
	NSX54	200	300	4	54	0	0.4	0.19	44.3	2.0

References

[1] Y.G. Du, L.A. Clark, A.H.C. Chan, Residual capacity of corroded reinforcing bars, Mag. Concr. Res. 57 (2005) 135–147, https://doi.org/10.1680/macr.2005.57.3.135.

[2] E. Moreno, A. Cobo, M.N. Gonzalez, Effect of corrosion degree on different steel ductility parameters, based on "equivalent steel" criterion, Int. J. Struct. Integr 7 (2016) 260–276, https://doi.org/10.1108/IJSI-09-2014-0048.

[3] D.V. Val, R.E. Melchers, Reliability of deteriorating RC slab bridges, J. Struct. Eng. 123 (1997) 1638–1644.

[4] ASCE. Seismic Evaluation and Retrofit of Existing Buildings: ASCE/SEI 41-17. Reston, VA: American Society of Civil Engineers; 2017. 10.1061/9780784414859.

[5] CEN. European Standard EN 1998-3:2005. Eurocode 8: Design of Structures for earthquake resistance - Part 3: Assessment and retrofitting of buildings. Incorporating corrigendum March 2010. European Committee for Standardization; 2005.

[6] N.S. Vu, B. Li, Seismic Performance Assessment of Corroded Reinforced Concrete Short Columns, J. Struct. Eng. 144 (2018) 04018018, https://doi.org/10.1061/(asce)st.1943-541x.0001994.

[7] N.S. Vu, B. Li, Seismic performance of flexural reinforced concrete columns with corroded reinforcement, ACI Struct. J. 115 (2018) 1253–1266, https://doi.org/10.14359/51702372.

[8] Y.-C. Ou, L.-L. Tsai, H.-H. Chen, Cyclic performance of large-scale corroded reinforced concrete beams, Earthq. Eng. Struct. Dyn. 41 (2012) 593–604, https://doi.org/10.1002/eqe.1145.

[9] Q. Li, D. Niu, Q. Xiao, X. Guan, S. Chen, Experimental study on seismic behaviors of concrete columns confined by corroded stirrups and lateral strength prediction, Constr. Build. Mater. 162 (2018) 704–713, https://doi.org/10.1016/j.conbuildmat.2017.09.030.

[10] J. Rodriguez, L.M. Ortega, J. Casal, Load carrying capacity of concrete structures with corroded reinforcement, Constr. Build. Mater. 11 (1997) 239–248, https://doi.org/10.1016/S0950-0618(97)00043-3.

[11] C.A. Apostolopoulos, G. Diamantogiannis, A.C. Apostolopoulos, Assessment of the Mechanical Behavior in Dual-Phase Steel B400C, B450C, and B500B in a Marine Environment, J. Mater. Civ. Eng. 28 (2016) 04015097, https://doi.org/10.1061/(asce)mt.1943-5533.0001271.

[12] C.A. Apostolopoulos, V.G. Papadakis, Consequences of steel corrosion on the ductility properties of reinforcement bar, Constr. Build. Mater. 22 (2008) 2316–2324, https://doi.org/10.1016/j.conbuildmat.2007.10.006.

[13] C. Goksu, A. Ilki, Seismic behavior of reinforced concrete columns with corroded deformed reinforcing bars, ACI Struct J. 113 (2016) 1053–1064, https://doi.org/10.14359/51689030.

[14] E. Moreno, A. Cobo, G. Palomo, M.N. González, Mathematical models to predict the mechanical behavior of reinforcements depending on their degree of corrosion and the diameter of the rebars, Constr. Build. Mater. 61 (2014) 156–163, https://doi.org/10.1016/j.conbuildmat.2014.03.003.

[15] Y.C. Ou, Y.T.T. Susanto, H. Roh, Tensile behavior of naturally and artificially corroded steel bars, Constr. Build. Mater. 103 (2016) 93–104, https://doi.org/10.1016/j.conbuildmat.2015.10.075.

[16] W. Zhang, X. Song, X. Gu, S. Li, Tensile and fatigue behavior of corroded rebars, Constr. Build. Mater. 34 (2012) 409–417, https://doi.org/10.1016/j.conbuildmat.2012.02.071.

[17] L. Yu, R. François, V.H. Dang, V. L'Hostis, R. Gagné, Structural performance of RC beams damaged by natural corrosion under sustained loading in a chloride environment, Eng. Struct. 96 (2015) 30–40, https://doi.org/10.1016/j.engstruct.2015.04.001.

[18] W. Jin, Effect of Corrosion on Bond Behavior and Bending Strength of Reinforced Concrete Beams, J Zhejiang Univ Sci 2 (2001) 298, https://doi.org/10.1631/jzus.2001.0298.

[19] A.A. Almusallam, A.S. Al-Gahtani, A.R. Aziz, Rasheeduzzafar, Effect of reinforcement corrosion on bond strength, Constr. Build. Mater. 10 (1996) 123–129, https://doi.org/10.1016/0950-0618(95)00077-1.

[20] M. Maslehuddin, I.M. Allam, G.J. Al-Sulaimani, A. Al-Mana, S.N. Abduljauwad, Effect of rusting of reinforcing steel on its mechanical properties and bond with concrete, ACI Mater. J. 87 (1990) 496–502, https://doi.org/10.14359/1902.

[21] J.G. Cabrera, Deterioration of concrete due to reinforcement steel corrosion, Cem. Concr. Compos. 18 (1996) 47–59, https://doi.org/10.1016/0958-9465(95)00043-7.

[22] L. Chung, J.H. Jay Kim, S.T. Yi, Bond strength prediction for reinforced concrete members with highly corroded reinforcing bars, Cem. Concr. Compos. 30 (2008) 603–611, https://doi.org/10.1016/j.cemconcomp.2008.03.006.

[23] H.S. Lee, T. Noguchi, F. Tomosawa, Evaluation of the bond properties between concrete and reinforcement as a function of the degree of reinforcement corrosion, Cem. Concr. Res. 32 (2002) 1313–1318, https://doi.org/10.1016/S0008-8846(02)00783-4.

[24] H. Yalciner, O. Eren, S. Sensoy, An experimental study on the bond strength between reinforcement bars and concrete as a function of concrete cover, strength

and corrosion level, Cem. Concr. Res. 42 (2012) 643–655, https://doi.org/10.1016/j.cemconres.2012.01.003.
[25] K. Soudki, T. Sherwood, Bond Behavior of Corroded Steel Reinforcement in Concrete Wrapped with Carbon Fiber Reinforced Polymer Sheets, J. Mater. Civ. Eng. 15 (2003) 358–370, https://doi.org/10.1061/(asce)0899-1561(2003)15:4(358).
[26] P.S. Mangat, M.S. Elgarf, Flexural strength of concrete beams with corroding reinforcement, ACI Struct. J. 96 (1999) 149–158, https://doi.org/10.14359/606.
[27] A.A. Torres-Acosta, S. Navarro-Gutierrez, J. Terán-Guillén, Residual flexure capacity of corroded reinforced concrete beams, Eng. Struct. 29 (2007) 1145–1152, https://doi.org/10.1016/j.engstruct.2006.07.018.
[28] A.K. El-Sayed, R.R. Hussain, A.B. Shuraim, Influence of stirrup corrosion on shear strength of reinforced concrete slender beams, ACI Struct. J. 113 (2016) 1223–1232, https://doi.org/10.14359/51689147.
[29] H. Li, J. Wu, Z. Wang, Shear performance of reinforced concrete beams with corroded stirrups strengthened with carbon fiber-reinforced polymer, ACI Struct. J. 113 (2016) 51–62, https://doi.org/10.14359/51687913.
[30] J. Xia, W. Jin, L. Li, Shear performance of reinforced concrete beams with corroded stirrups in chloride environment, Corros. Sci. 53 (2011) 1794–1805, https://doi.org/10.1016/j.corsci.2011.01.058.
[31] L. Yu, R. François, R. Gagné, Mechanical performance of deep beams damaged by corrosion in a chloride environment, Eur. J. Environ. Civ. Eng. 22 (2018) 523–545, https://doi.org/10.1080/19648189.2016.1210033.
[32] C. Higgins, W.C. Farrow, Tests of reinforced concrete beams with corrosion-damaged stirrups, ACI Struct J. 103 (2006) 133–141, https://doi.org/10.14359/15094.
[33] A. Imam, A.K. Azad, Prediction of residual shear strength of corroded reinforced concrete beams, Int. J. Adv. Struct. Eng. 8 (2016) 307–318.
[34] C.A. Juarez, B. Guevara, G. Fajardo, P. Castro-Borges, Ultimate and nominal shear strength in reinforced concrete beams deteriorated by corrosion, Eng. Struct. 33 (2011) 3189–3196.
[35] Z.H. Lu, H. Li, W. Li, Y.G. Zhao, Z. Tang, Z. Sun, Shear behavior degradation and failure pattern of reinforced concrete beam with chloride-induced stirrup corrosion, Adv. Struct. Eng. 22 (2019) 2998–3010, https://doi.org/10.1177/1369433219855917.
[36] X. Xue, H. Seki, Y. Song, Shear behavior of RC beams containing corroded stirrups, Adv. Struct. Eng. 17 (2014) 165–178, https://doi.org/10.1260/1369-4332.17.2.165.
[37] Y. Zhao, W. Jin, Analysis on shearing capacity of concrete beams with corroded stirrups, J. Zhejiang Univ. (Engineering Sci 42 (2008) 19–23.
[38] X. Li, Z.H. Zhao, Y.S. Liang, H.L. Lv, Cyclic behaviour of earthquakeand corrosion-damaged RC columns, Mag. Concr. Res. 68 (2016) 1166–1182, https://doi.org/10.1680/jmacr.16.00155.
[39] H. Zheng, S. Zheng, Y. Zhang, Y. Cai, M. Ming, J. Zhou, Experimental Investigation on Seismic Behaviours of Reinforced Concrete Columns under Simulated Acid Rain Environment, Adv. Civ. Eng. 2020 (2020), https://doi.org/10.1155/2020/3826062.
[40] S.S. Zheng, L. Dong, H. Zuo, Q. Qin, W. Liu, Q. Li, Experimental investigation on seismic behaviors of corroded RC frame columns in artificial climate, J. Build. Struct. 39 (2018) 28–36.
[41] A. Meda, S. Mostosi, Z. Rinaldi, P. Riva, Experimental evaluation of the corrosion influence on the cyclic behaviour of RC columns, Eng. Struct. 76 (2014) 112–123, https://doi.org/10.1016/j.engstruct.2014.06.043.
[42] A. Guo, H. Li, X. Ba, X. Guan, H. Li, Experimental investigation on the cyclic performance of reinforced concrete piers with chloride-induced corrosion in marine environment, Eng. Struct. 105 (2015) 1–11, https://doi.org/10.1016/j.engstruct.2015.09.031.
[43] K.Y. Dai, C. Liu, D.G. Lu, X.H. Yu, Experimental investigation on seismic behavior of corroded RC columns under artificial climate environment and electrochemical chloride extraction: A comparative study, Constr. Build. Mater. 242 (2020), 118014, https://doi.org/10.1016/j.conbuildmat.2020.118014.
[44] A. Karimipour, M. Edalati, Retrofitting of the corroded reinforced concrete columns with CFRP and GFRP fabrics under different corrosion levels, Eng. Struct. 228 (2021), 111523, https://doi.org/10.1016/j.engstruct.2020.111523.
[45] A.S. Rajput, U.K. Sharma, Performance of aged reinforced concrete columns under simulated seismic loading, Struct. Concr 20 (2019) 1123–1136, https://doi.org/10.1002/suco.201800235.
[46] H. Funaki, T. Yamakawa, K. Nakada, Experimental studies on durability and seismic performance of real-scaled RC columns exposed at a coastal area in okinawa, J. Struct. Constr. Eng. (2011).
[47] Y.C. Ou, N.D. Nguyen, Influences of location of reinforcement corrosion on seismic performance of corroded reinforced concrete beams, Eng. Struct. 126 (2016) 210–223, https://doi.org/10.1016/j.engstruct.2016.07.048.
[48] Y.-C. Ou, H.-H. Chen, Cyclic Behavior of Reinforced Concrete Beams with Corroded Transverse Steel Reinforcement, J. Struct. Eng. 140 (2014) 04014050, https://doi.org/10.1061/(asce)st.1943-541x.0000932.
[49] Y. Ma, Y. Che, J. Gong, Behavior of corrosion damaged circular reinforced concrete columns under cyclic loading, Constr. Build. Mater. 29 (2012) 548–556, https://doi.org/10.1016/j.conbuildmat.2011.11.002.
[50] Z. Yuan, C. Fang, M. Parsaeimaram, S. Yang, Cyclic Behavior of Corroded Reinforced Concrete Bridge Piers, J. Bridg. Eng. 22 (2017) 04017020, https://doi.org/10.1061/(asce)be.1943-5592.0001043.
[51] D. Li, R. Wei, F. Xing, L. Sui, Y. Zhou, W. Wang, Influence of Non-uniform corrosion of steel bars on the seismic behavior of reinforced concrete columns, Constr. Build. Mater. 167 (2018) 20–32, https://doi.org/10.1016/j.conbuildmat.2018.01.149.
[52] S.Y. Yang, X.B. Song, H.X. Jia, X. Chen, L.X. La, Experimental research on hysteretic behaviors of corroded reinforced concrete columns with different maximum amounts of corrosion of rebar, Constr. Build. Mater. 121 (2016) 319–327, https://doi.org/10.1016/j.conbuildmat.2016.06.002.
[53] J. Cairns, Y. Du, D. Law, Residual bond strength of corroded plain round bars, Mag. Concr. Res. 58 (2006) 221–231, https://doi.org/10.1680/macr.2006.58.4.221.
[54] W. Zhu, R. François, D. Cleland, D. Coronelli, Failure mode transitions of corroded deep beams exposed to marine environment for long period, Eng. Struct. 96 (2015) 66–77, https://doi.org/10.1016/j.engstruct.2015.04.004.
[55] C. Zeng, J.H. Zhu, C. Xiong, Y. Li, D. Li, J. Walraven, Analytical model for the prediction of the tensile behaviour of corroded steel bars, Constr. Build. Mater. 258 (2020), 120290, https://doi.org/10.1016/j.conbuildmat.2020.120290.
[56] Y.G. Du, L.A. Clark, A.H.C. Chan, Effect of corrosion on ductility of reinforcing bars, Mag. Concr. Res. 57 (2005) 407–419.
[57] K. Bhargava, A.K. Ghosh, Y. Mori, S. Ramanujam, Corrosion-induced bond strength degradation in reinforced concrete-Analytical and empirical models, Nucl. Eng. Des. 237 (2007) 1140–1157, https://doi.org/10.1016/j.nucengdes.2007.01.010.
[58] C.O. Orangun, J.O. Jirsa, J.E. Breen, Reevaluation of Test Data on Development Length and Splices, ACI J. 74 (1977) 114–122, https://doi.org/10.14359/10993.
[59] ACI 318. ACI 318-19 Building Code Requirements for Structural Concrete and Commentary. 2019. 10.14359/51716937.
[60] GB50010-2002. Code for Design of Concrete Structures (in Chinese). Beijing, China: China Building Industry Press; 2002.
[61] ACI-ASCE Committee 326. Shear and diagonal tension. Report of the ACI-ASCE Committee 326; 1962.
[62] X. Xue, H. Seki, Influence of longitudinal bar corrosion on impact behavior of RC beams, J. Adv. Concr. Technol. 8 (2010) 145–156, https://doi.org/10.1617/s11527-015-0741-0.
[63] E.A. Opabola, K.J. Elwood, Seismic assessment of reinforced concrete columns with short lap splices, Earthq. Spectra 875529302199483 (2021), https://doi.org/10.1177/8755293021994834.
[64] V.V. Bertero, E.P. Popov, Hysteretic behavior of ductile moment-resisting reinforced concrete frame components, University of California, College of Engineering, 1975.
[65] E.A. Opabola, K.J. Elwood, S. Oliver, Deformation capacity of reinforced concrete columns with smooth reinforcement, Bull. Earthq. Eng. 17 (2019) 2509–2532, https://doi.org/10.1007/s10518-018-00540-w.
[66] Y. Auyeung, P. Balaguru, L. Chung, Bond behavior of corroded reinforcement bars, ACI Struct. J. 97 (2000) 214–220, https://doi.org/10.14359/826.
[67] G.J. Al-Sulaimani, M. Kaleemullah, I.A. Basunbul, Rasheeduzzafar, Influence of corrosion and cracking on bond behavior and strength of reinforced concrete members, ACI Struct J. 87 (1990) 220–231, https://doi.org/10.14359/2732.